STUDIES ON CONVERTER FED DC-DRIVES

A Thesis Submitted
in Partial Fulfilment of the Requirements
for the Degree of
MASTER OF TECHNOLOGY

By
P B ANJANEYULU

to the
DEPARTMENT OF ELECTRICAL ENGINEERING
INDIAN INSTITUTE OF TECHNOLOGY, KANPUR
JULY, 1979

EE-1979-M-ANJ-STU

TO

MY FATHER

CERTIFICATE

Certified that this work "Studies on Converterfed D.C. Drives" by P.B. Anjaneyulu is carried out under our supervision and is not submitted elsewhere for a degree.

Dr. G K. Dubey
Professor

Dr. S.S. Prabhu
Professor

Department of Electrical Engineering
Indian Institute of Technology
Kanpur

ABSTRACT

This thesis deals with some aspects of converter-fed dc motor. A novel versatile firing scheme has been developed for converter control schemes. A new method for the calculation of filter inductance which eliminates discontinuous conduction and keeps the ripple within permissible limits is presented. A simple method for the design of controllers is derived which eliminates the ripple instability as well as runaway instability. System has been digitally simulated and compared with experimental results. An experimental investigation of autoadaptive controller has been carried out.

ACKNOWLEDGEMENTS

I wish to express my deep sense of gratitude to Dr G K Dubey and Dr. S S Prabhu for their able and dynamic guidance. I wish to thank Dr. S R. Doradla, Mr C Radhakrishna and Mr S S Bhatnagar for useful discussions with them I am grateful to Mr.N.D Sharma for his cooperation I wish to thank Mr D V S. Rao, Mr N Gopinath, Mr R V Ghalam, Mr Balachandar, Mr B R K Reddy, Mr S.V S Rao and all my friends for their help at various stages

I am also thankful to Mr. K N Tewari for his excellent typing

P B. Anjaneyulu

NOMENCLATURE

E_d	motor back emf, V.
E_m	peak value of ac input voltage, V
i_a	instantaneous armature current, Amp.
i_p	instantaneous armature current in p u.
WN	speed in p.u
TN	torque in p u.
I_m	$E_m/\sqrt{R_a^2 + w^2 L_a^2}$, Amp.
L_a	total inductance in armature circuit, H
R_a	armature resistance, ohms
ω	speed in radians/sec.
RF	ripple factor
α_f	triggering angle, deg.
β	extinction angle, deg.
γ	angle at which instantaneous ac supply voltage is equal to back emf of motor, deg.
ψ	$\tan^{-1}(wL_a/R_a)$, rad.
w	angular frequency of ac supply voltage, rad/sec.
Ua	armature voltage, V
K_v	back emf constant
K_t	torque constant
J	moment of inertia
B	viscous friction constant
V_m	maximum control voltage (12V)
V_{ref}	speed reference voltage

K_{s1}	speed controller gain
τ_a	speed controller time constant
K_1	current controller gain
K_{f1}	current transducer gain
K_{fs}	speed transducer gain
T_l	Load torque
ω_∞	steady state speed, rad/sec.
$I_{a\infty}$	steady state current, Amp.
$\alpha_{f\infty}$	steady state firing angle, rad

CONTENTS

CHAPTER I

INTRODUCTION

DC drives are widely used in applications requiring variable speed, good speed regulation, frequent starting and reversing. Some important applications are in rolling mills, paper mills, minewinder, machine tools and traction. DC motors controlled by thyristor converters have become the most popular form of industrial variable speed edrive. The thyristor converter has the advantages of high reliability, efficiency and power gain coupled with its small size and fast response. However there are certain disadvantages like high ripple content in the motor armature current and generation of harmonics in the ac supply. The present thesis deals with certain aspects of converter controlled dc drive employing separately excited dc motor.

1.1 CONVERTER FIRING CONTROL CIRCUIT

There are many circuits available in the literature to obtain time delay for phase angle control of thyristors. UJT and monostable circuits have been commonly used in the past [1-3]. These suffer from the following limitations.

1. Monostable circuits are sufficiently sensitive for stray pulses which results in false triggering [2].
2. The relationship between control voltage and time delay is not linear [2].

3. There is a finite recovery time and it increases for large time delay.

The UJT time delay circuit [1] is quite stable in operation. However, the shape of the output pulse is dependent on the load into which the timing capacitor discharges through the emitter of UJT. For sustained triggering of SCRs, the UJT output pulse is to be further processed using bistable and monostable circuits. This makes the system more sensitive to stray pulses. For automatic control of the time delay, the charging current of the capacitor is controlled [1]. In such cases the delay cannot be reduced below a fixed minimum which depends on the maximum allowable charging current. This minimum value increases for circuits designed for large time delay.

Arockiasamy and Doriapandy [4] have described a circuit which overcomes the above limitations. This circuit uses two separate channels, one for each half-cycle of the mains voltage. The circuit has the limitation that an exact 180° phase difference between the firing pulses sent to a pair of thyristors in the same mains phase, conducting alternately in the two halves of the mains supply cannot be realised. Yair and Steinkoler [5] have removed this limitation. Their circuit is however not versatile in the sense that it cannot be used for many converter control operations.

The circuit proposed in Chapter II of the thesis is simple and suitable for many converter operations such as i) fully controlled operation ii) fully controlled operation with half controlled characteristics [6] iii) sequence control [7] iv) symmetrical pulse width modulation with one pulse per half cycle [8] and v) asymmetrical triggering control [7]. The same principle can be extended to 3-phase ac voltage controller [9] and 3-phase thyristor bridge converter operation. The circuit is stable and immune to noise and stray pulses.

1 2 SELECTION OF FILTER INDUCTANCE

Mehta and Mukopadhyay [10] have described a method for the calculation of inductance so that discontinuous conduction does not occur during normal steady state operation. Their method, however, neglects the armature circuit resistance and does not account for the nature of the load torque-speed characteristic. Subbaiah and Palanichamy [15] have extended this method to account for armature circuit resistance drop, however, they have also not accounted for nature of load torque-speed curves. An elegant method for the calculation of optimum value of inductance for fully controlled and half controlled converters taking the nature of speed torque characteristics of the load has been presented. Monograms have been given in terms of normalised variables. A flowchart has also been given for the calculation of monograms. These can

be used to obtain an optimum value of inductance for any motor controlled by fully controlled or half controlled converter.

1 3 STABILITY ANALYSIS AND DESIGN OF CLOSED LOOP CONVERTER CONTROLLED DC MOTOR

Krishnan and Ramaswamy [16] have designed the controller parameters using symmetric optimum method. Thyristor converter has been approximated as a constant gain amplifier. Farag and Malick [22] have described the stability analysis taking the dc motor as a first order system, neglecting the armature time constant. In the present work (Chapter 4), dc motor has been considered as a second order system and the nonlinearity of the thyristor converter has been taken into account. State space techniques have been used for the design of controllers to ensure that the system is locally stable. A method employing Popov's criteria has been presented to test the system stability in the large.

1 4 STUDY OF AUTO-ADAPTIVE CONTROLLER AND DIGITAL SIMULATION OF CONVERTER CONTROLLED DC MOTOR IN CLOSED-LOOP

Abbot and Wheeler [21] suggested an adaptive controller for the dc motor drive by interpreting the results of the analog computer simulation. In the present work dc drive with auto-adaptive controller has been built and its performance has been experimentally investigated (Chapter 4). The system with

the adaptive controller is also simulated on a digital computer. Simulation results have been compared with those obtained experimentally.

CHAPTER II

A NOVEL VERSATILE PULSE DELAY CIRCUIT FOR CONVERTER CONTROL

A simple and versatile firing circuit suitable for many converter operations such as (i) fully controlled operation (ii) fully controlled operation with half-controlled characteristics [6] (iii) sequence control [7] (iv) symmetrical pulse width modulation with one pulse per half cycle [8] and (v) asymmetrical triggering control [7] is described here It can be extended to 3-phase ac voltage controller [9] and 3-phase thyristor bridge converter operation. The circuit is stable and immune to noise and stray pulses.

2 1 PROPOSED SCHEME

The block diagram of the proposed scheme is shown in Fig 2 1. The basic waveforms are shown in Fig.2.3.

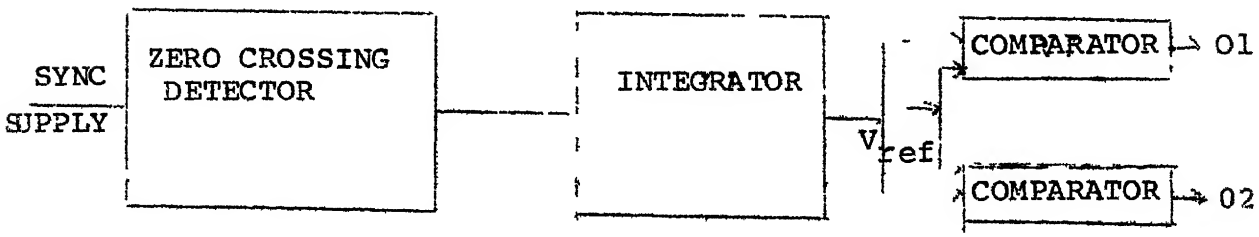

Fig.2.1 Proposed Scheme.

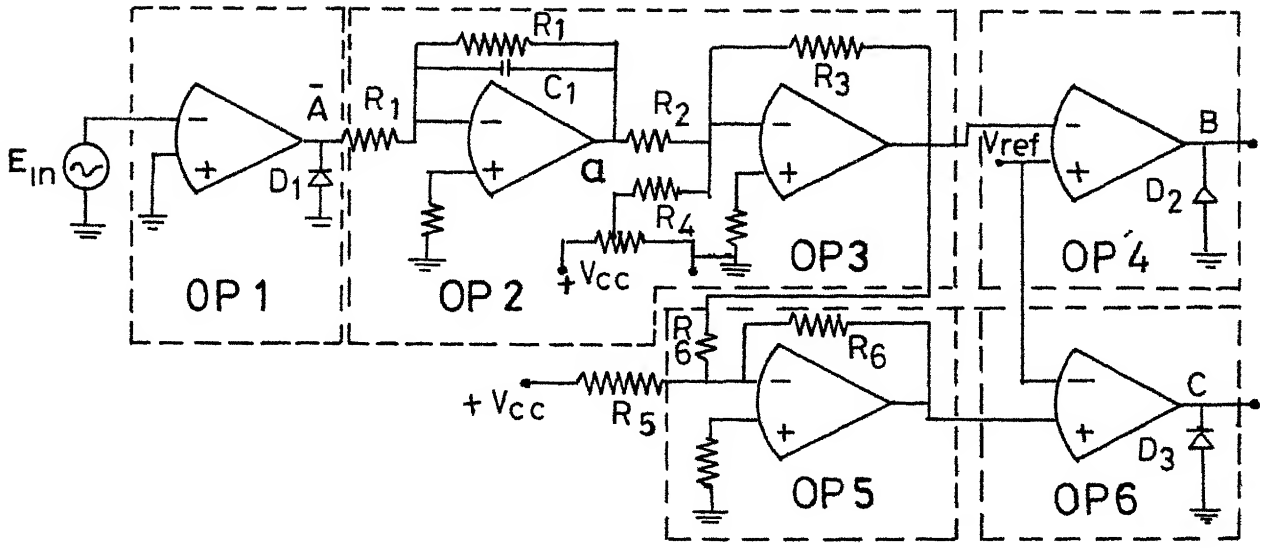

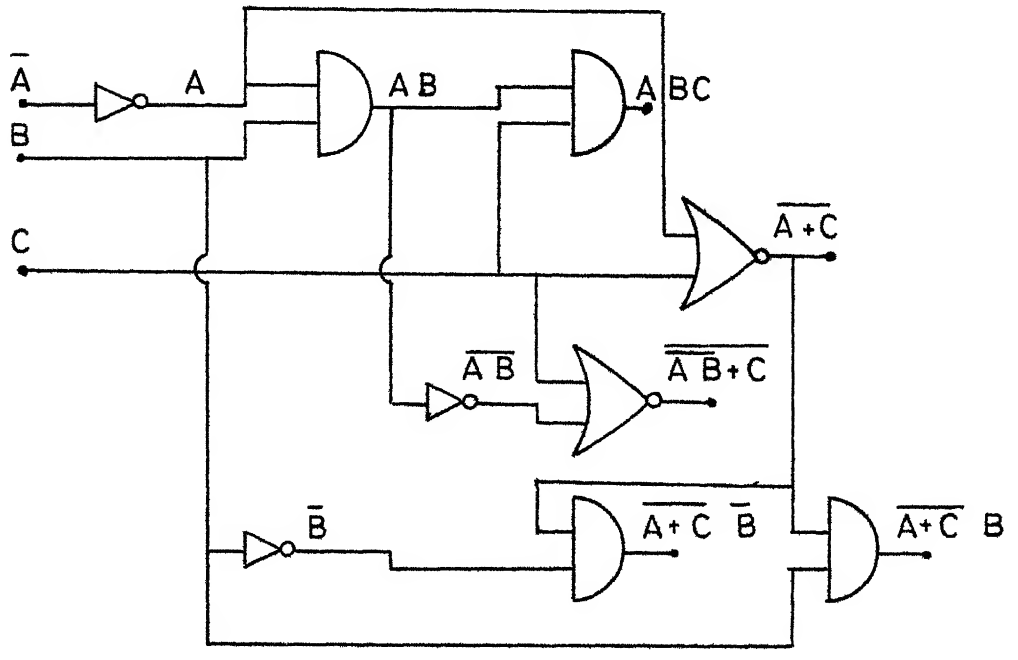

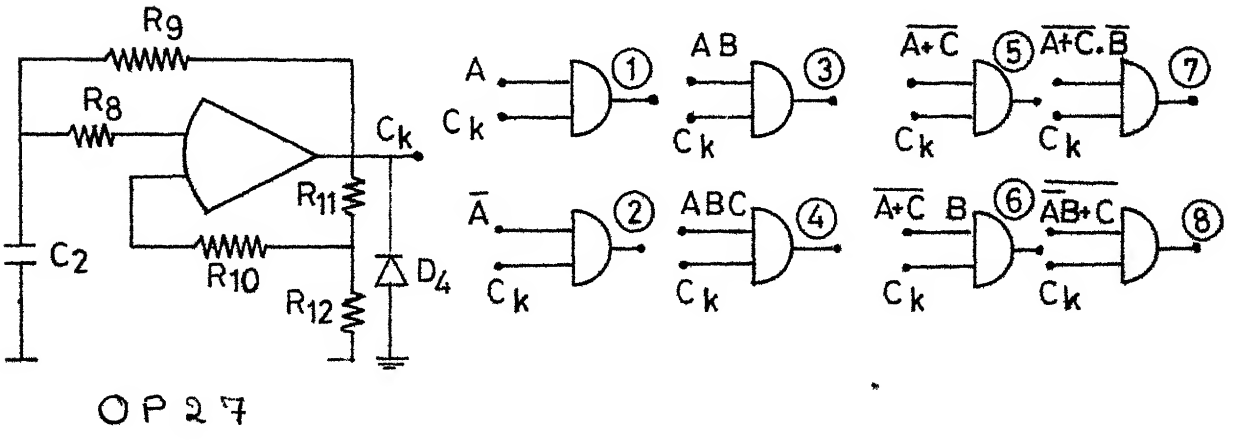

Fig 2·2 Firing circuit

The principle of operation is based on converting the synchronisation supply to a square wave (Fig. 2.3b). A triangular wave TR1 (Fig.2.3d) is generated by integrating the square wave TR1 is compared with reference voltage V_R to generate a pulse B of duration α to $2\pi-\alpha$ as shown in Fig.2.3e. TR1 is also inverted and compared with reference voltage V_R. The pulse C of duration from $\pi-\alpha$ to $\pi+\alpha$ is obtained as shown in Fig.2.3g. The pulses A, B and C can now be processed to get the pulses of any of the following durations. (1) 0 to π (2) π to 2π (3) α to π (4) $\pi-\alpha$ to π (5) $\pi+\alpha$ to 2π (6) $2\pi-\alpha$ to 2π (7) α to $\pi-\alpha$ (8) $\pi+\alpha$ to $2\pi-\alpha$. This makes the circuit versatile and can be adapted to any converter control mentioned above.

2.2 REALISATION

The circuit diagram is shown in Fig 2.2. The waveforms at the output of each stage are shown in Fig 2 3. OP-1 converts the synchronisation supply to a square wave as shown in Fig 2.3b. OP-2 integrates the input $\bar{A}$ of Fig.2.2. The initial condition of the system will die away due to the feedback resistance R_1 of the amplifier OP-2 of Fig.2 2. But it introduces the dc level at the output (Fig. 2.3c). The waveform as shown in Fig 2 3d is obtained by the dc level shifter OP-3 which works as an amplifier. This is compared with reference voltage V_R and the waveform B as shown in Fig 2.3e is obtained. The waveform TR1 of Fig.2.3 is inverted

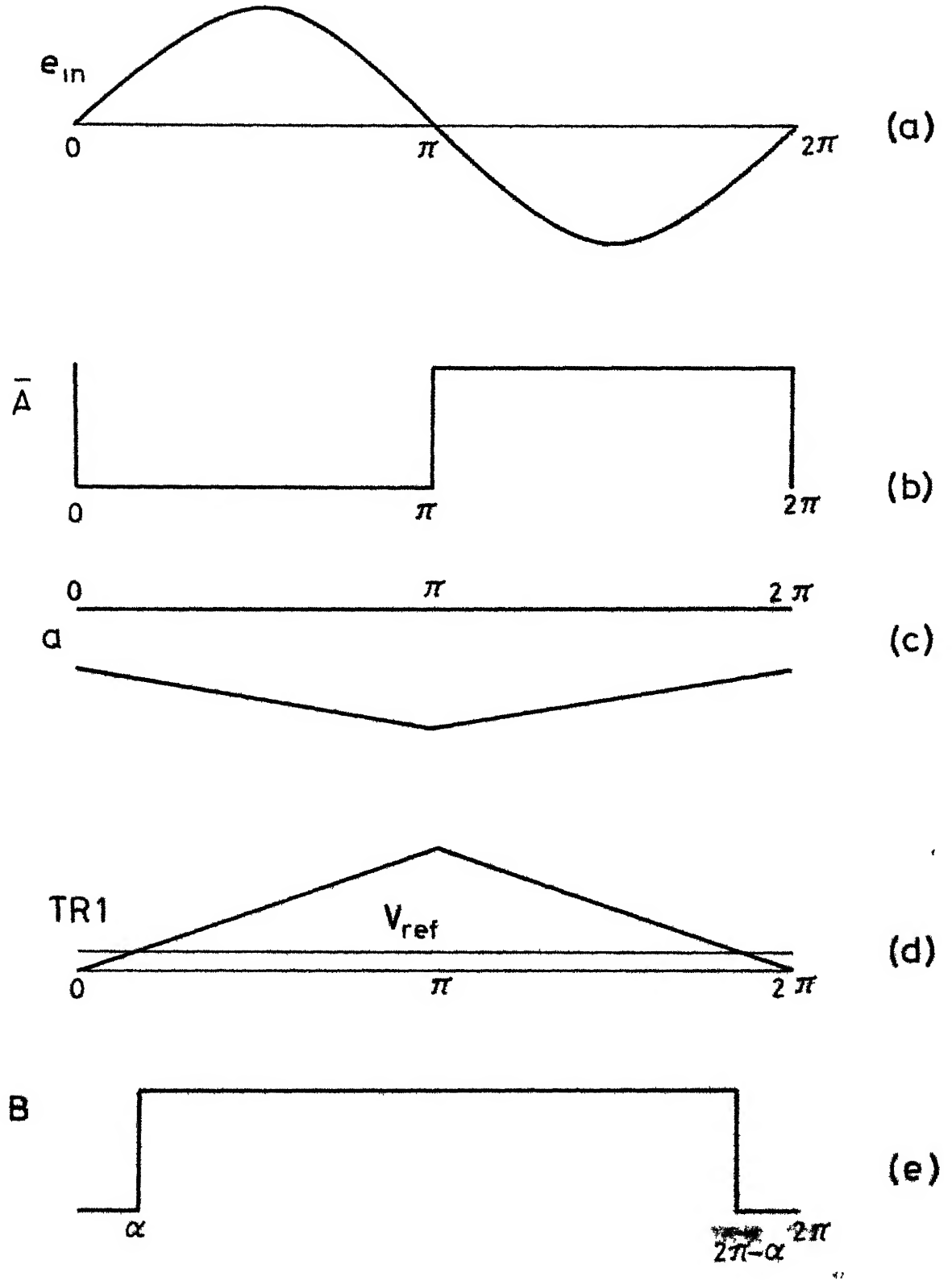

Fig.2·3 Waveforms at each stage of Fig.2·2

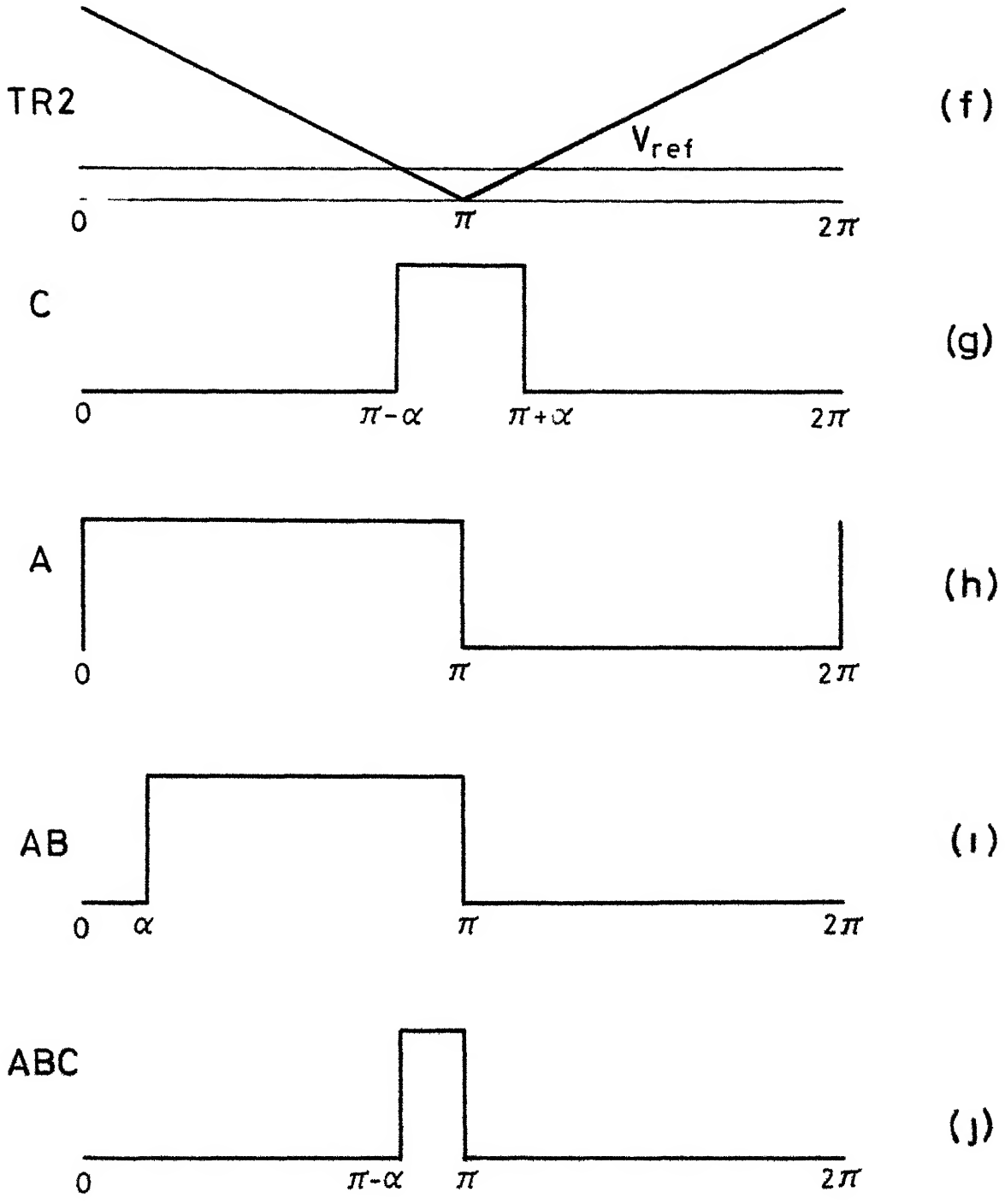

Fig. 2·3 Contd.

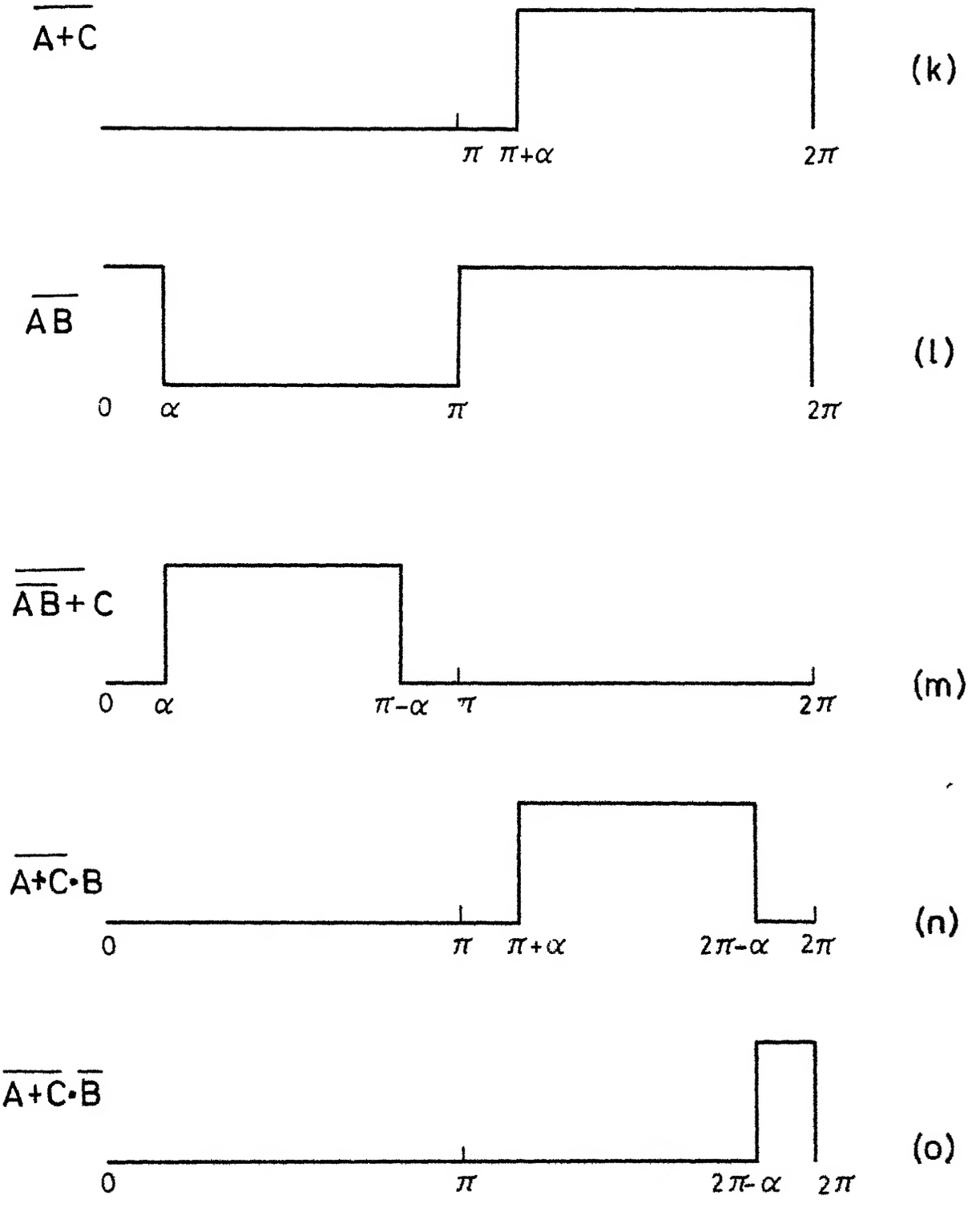
$\overline{A+C}$
(k)
π $\pi+\alpha$ 2π
$\overline{AB}$
(l)
0 α π 2π
$\overline{\overline{AB}+C}$
(m)
0 α $\pi-\alpha$ π 2π
$\overline{A+C\cdot B}$
(n)
0 π $\pi+\alpha$ $2\pi-\alpha$ 2π
$\overline{A+C}\cdot\overline{B}$
(o)
0 π $2\pi-\alpha$ 2π

Fig. 2·3 Contd.

and level shifted by OP-5 of Fig.2.2 as shown in Fig 2.3f. This is compared with reference voltage V_R. The waveform C as shown in Fig.2.3g is obtained. The waveforms A, B and C are processed to obtain the waveforms as shown in Figs.2.3g to 2 3o. OP-7 of Fig.2.2 is used as a clock of frequency 5 KHz. The output is gated with the waveforms of Figs 2.3h to 2 3o. The gated output drives the pulse amplifier which is used to trigger the thyristors.

2.3 APPLICATIONS

In all the applications, though the explanation of circuit operation is given for continuous current case only, the circuit is applicable in discontinuous case also.

(i) Fully controlled operation

The power circuit bridge is shown in Fig.2.4a. The output waveform E_{out} of Fig.2.4a is shown in Fig. 2.5a. During the period from α to $\pi+\alpha$, thyristors T_1 and T_2 are ON, being triggered by the clocked waveform of Fig.2.3i. The thyristors T_3 and T_4 are triggered by the clocked output of Fig. 2.3K.

(ii) Fully controlled bridge with half controlled characteristics.

The power circuit is shown in Fig.2.4a. The output waveform E_{out} is shown in Fig.2.5b. During the positive half cycle, the thyristors T_1 and T_2 are ON from period α to π radians. Thyristor T_1 is triggered by the waveform

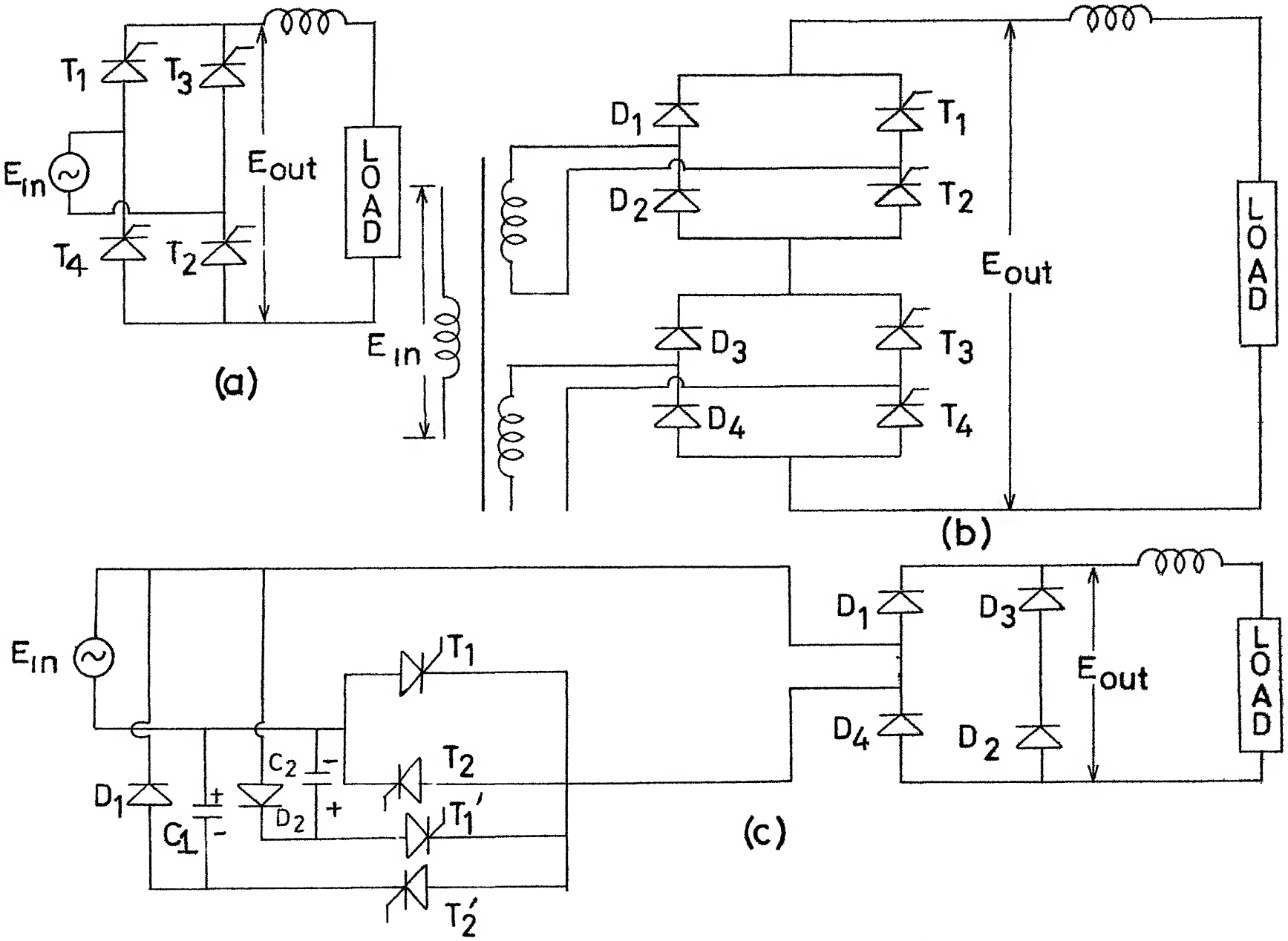

Fig.2·4 Power circuits

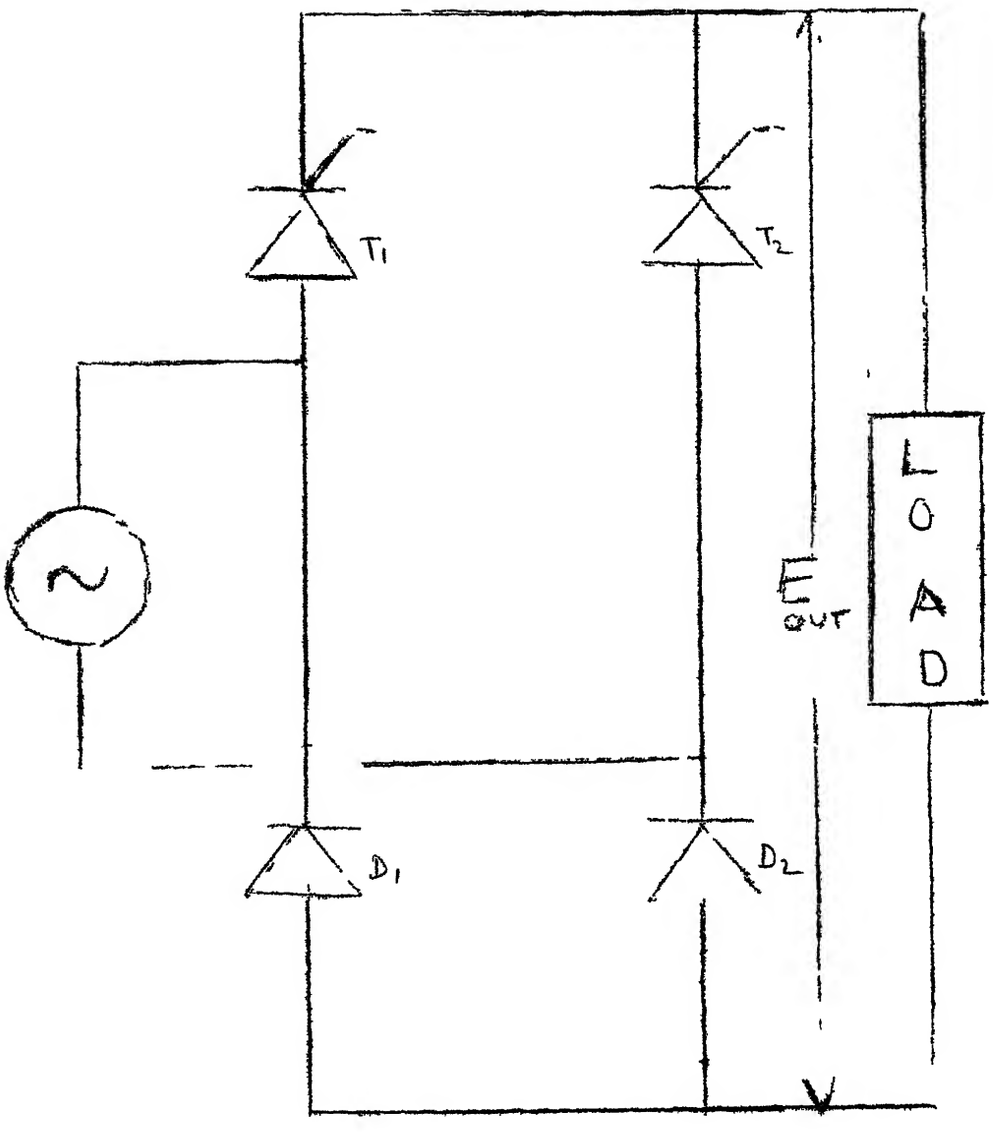

FIG 2 4d

shown in Fig.2 3h and thyristor T_2 is triggered by the clocked output of the waveform shown in Fig. 2.3i. During the negative half-cycle, at the instant π , thyristor T_3 is triggered by the clocked output of the waveform shown in Fig. 2.3b If the current is continuous, the part of the waveform CD of Fig.2 5b is obtained. At the instant D, thyristor T_4 is triggered by the waveform shown in Fig 2 3i. The part of the waveform EF of Fig.2.5b is obtained. The part GA is obtained by the triggering of thyristor T_1 by the clocked output of the waveform shown in Fig.2.3b. Thus it operates as a fully coitrolled bridge with half controlled characteristics.

(iii) Sequence control

The bridge circuit is shown in Fig.2.4b. The output voltage waveform E_{out} is shown in Fig.2.5c. The part of the waveform AB is obtained by the conduction of thyristor T_2 triggered by the clocked output waveform shown in Fig.2.3h and by the diodes D_1, D_3 and D_4. At the instant α , T_4 is triggered by the waveform shown in Fig.2.3i, and the part of the waveform CD is obtained. During the negative half-cycle of the supply, at the instant D, thyristor T_1 is triggered by the clocked output of the waveform shown in Fig.2.3b. The part of the waveform DE is obtained by the conduction of the diodes D_3, D_4 and D_4. At an angle $\pi+\alpha$, thyristor T_3 is triggered by the clocked output of the

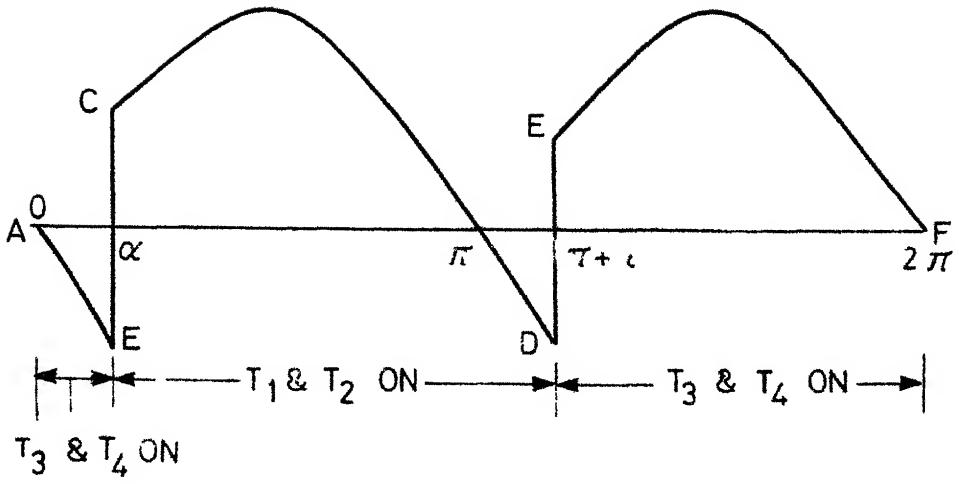

(a)

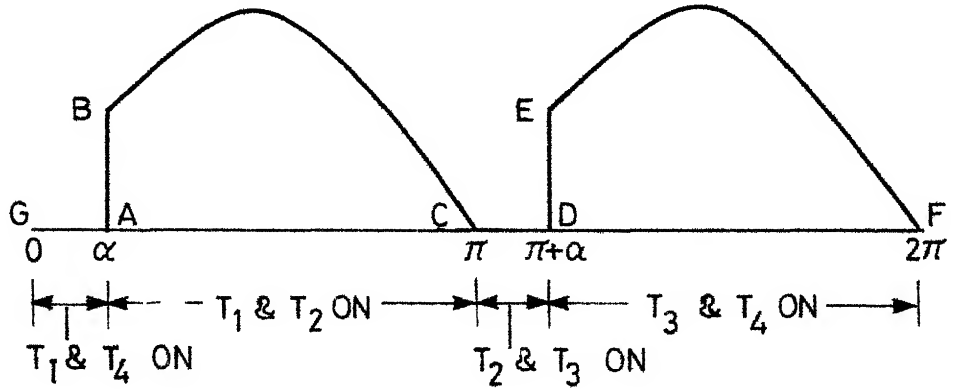

(b)

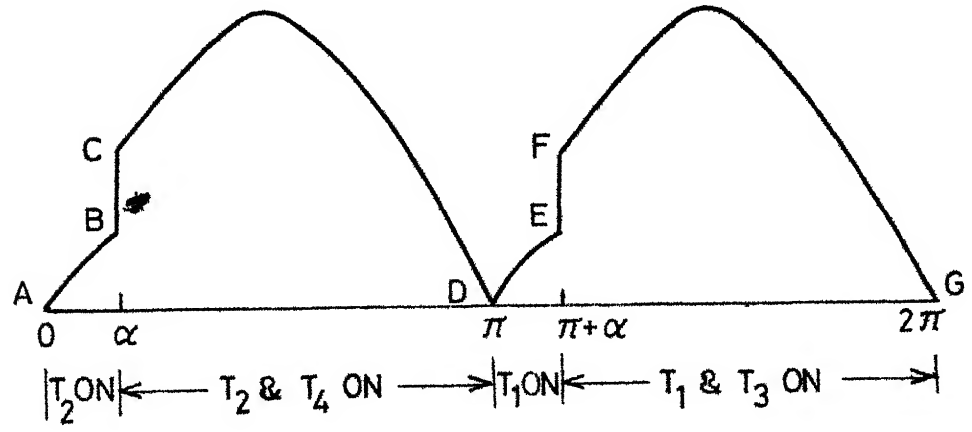

(c)

Fig. 2 5 Output waveforms of Fig. 2·4

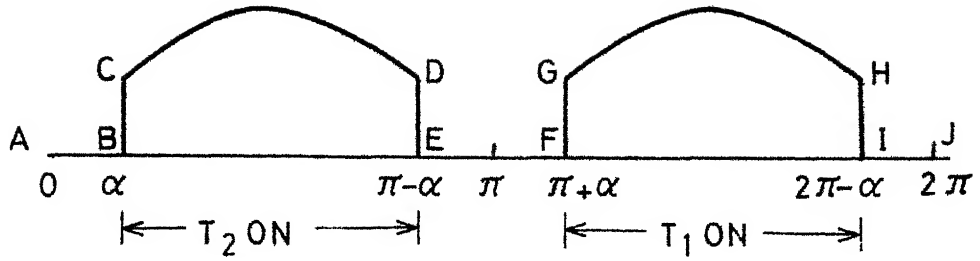

(d)

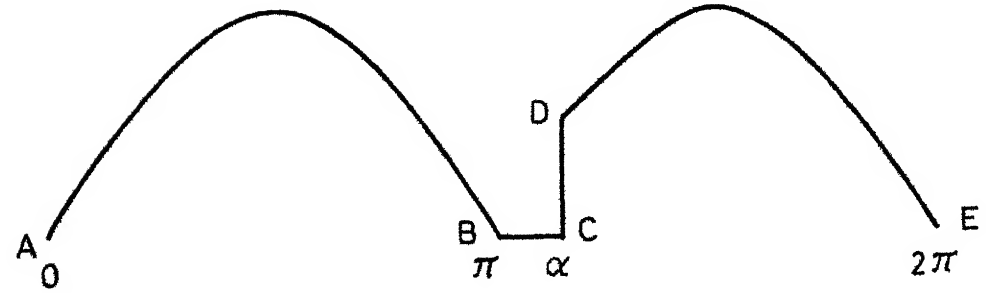

(e)

Fig. 2·5 Contd.

waveform shown in Fig.2.3k. The part of the waveform FG is obtained by the conduction of thyristors T_1 and T_3, Diodes D_2 and D_4. Thus the waveform ABCDEFG is obtained.

iv) Symmetrical pulse width modulation with single pulse per half cycle.

The power circuit is shown in Fig.2.4c The output voltage waveform E_{out} is shown in Fig 2.5d. During the positive half cycle, at the instant B, thyristor T_2 is triggered by the clocked output of the waveform shown in Fig. 2.3m. At the instant E, T_2 is forced commutated by capacitor C_1 (charged in the previous half cycle) by the triggering of the thyristor T_2' which is turned ON by the clocked output of the waveform shown in Fig. 2.3j. During the negative half cycle, at the instant F, thyristor T_1 is triggered ON by the waveform shown in Fig. 2.3n. At the instant I, T_1 is forced commutated by the turning ON of of thyristor T_1' which is being triggered by the clocked output of the waveform shown in Fig.2.3o. Thus the waveform ABCDEFGHIJ is obtained.

(v) Asymmetrical triggering.

The power circuit is shown in Fig.2.4d. The output voltage waveform is shown in Fig.2.5e. During the positive half cycle, at the instant A, thyristor T_1 is triggered by the clocked output of the waveform shown in Fig. 2.3h. At the instant C, T_2 is triggered by the clocked output waveform

shown in Fig. 2 3k. Thus the wave-form ABCDE of Fig.2.5e is obtained.

The basic approach can be employed for 3-phase ac voltage controller and 3-phase bridge configuration.

CHAPTER III

CALCULATION OF FILTER INDUCTANCE

3.1 INTRODUCTION

Fig. 3.1 shows the basic circuit for the converter controlled dc separately excited motor. The freewheeling diode FD, shown in dotted lines, is for half controlled operation. Various modes of operation have been described by Mehta and Mukopadhyay [10]. Typical armature current waveforms in different modes are shown in Figs. 3.2(a) and 3.2(b) The armature current is not smooth dc but has an ac ripple superimposed on dc component Since the motor induced emf is a function of field flux and speed, at high speeds and low average armature currents (or low load torques) the current may become zero as shown in Figs. 3.2(b) and 3 2(d) The motor is then said to operate under the discontinuous current mode. Large ac ripple and discontinuous conduction are not desirable as they adversely affect the commutation of the machine and increase the losses, thus reducing the efficiency and derating the motor [11,12]. Furthermore, discontinuous conduction makes the speed regulation poor and transient response slow [13].

The discontinuous conduction can be eliminated and ac ripple reduced by increasing the electrical time constant of the machine by connecting an external inductance in the armature circuit. This improves the speed regulation.

It also has the beneficial effect on the speed drop under impact loading condition [12] However, the addition of external inductance in the armature circuit results in reduction in efficiency (due to losses in the inductance), increase in cost, weight, size and deterioration of transient response [13].

If inductance is absolutely necessary, as is the case with separately excited motor, its value should be just enough to eliminate discontinuous conduction and keep the ac ripple within acceptable limits. This will ensure that these performance objectives are achieved with minimal deterioration of transient response and introduction of other adverse effects mentioned above.

3 2 MODES OF OPERATION AND PERFORMANCE EQUATIONS

It is assumed that a) the thyristors and diodes are ideal switches b) the resistance and inductance of the motor armature are constant c) the commutation overlap due to source inductance is negligible d) during a given steady state condition, the motor speed is constant. (Since the mechanical time constant of the motor is very large compared to the half cycle period of the supply, the fluctuation in speed during this period is negligible). The equivalent circuits of converter controlled dc motor under three different modes of operation [10] are described below.

Mode 1 In this mode (Figs. 3.2b , 3.2f), the current is discontinuous and the earliest instant at which the thyristor can be fired is γ where $\gamma = \sin^{-1} E_b/E_m$.

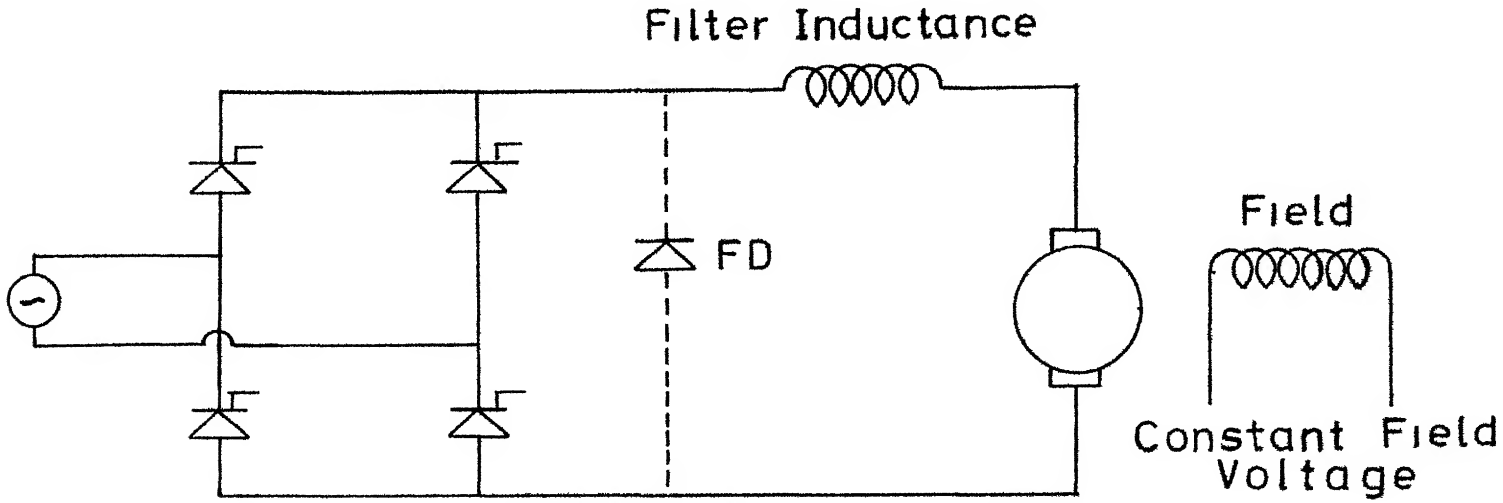

Fig 3 1 Converter controlled D C separately excited motor

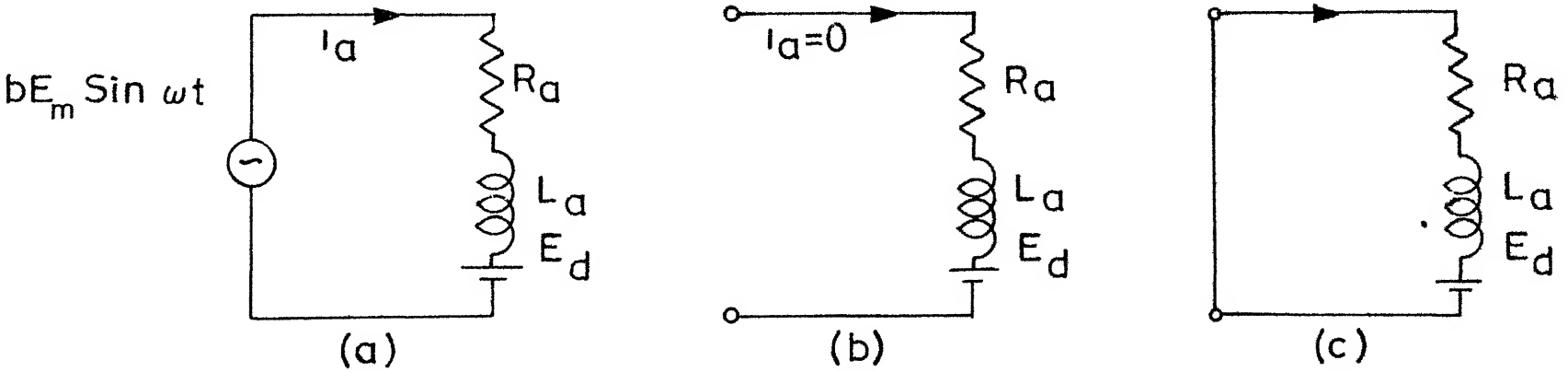

Fig 3 3 Equivalent circuits (a) Thyristor conduction interval
(b) Zero current interval (c) Free wheeling interval

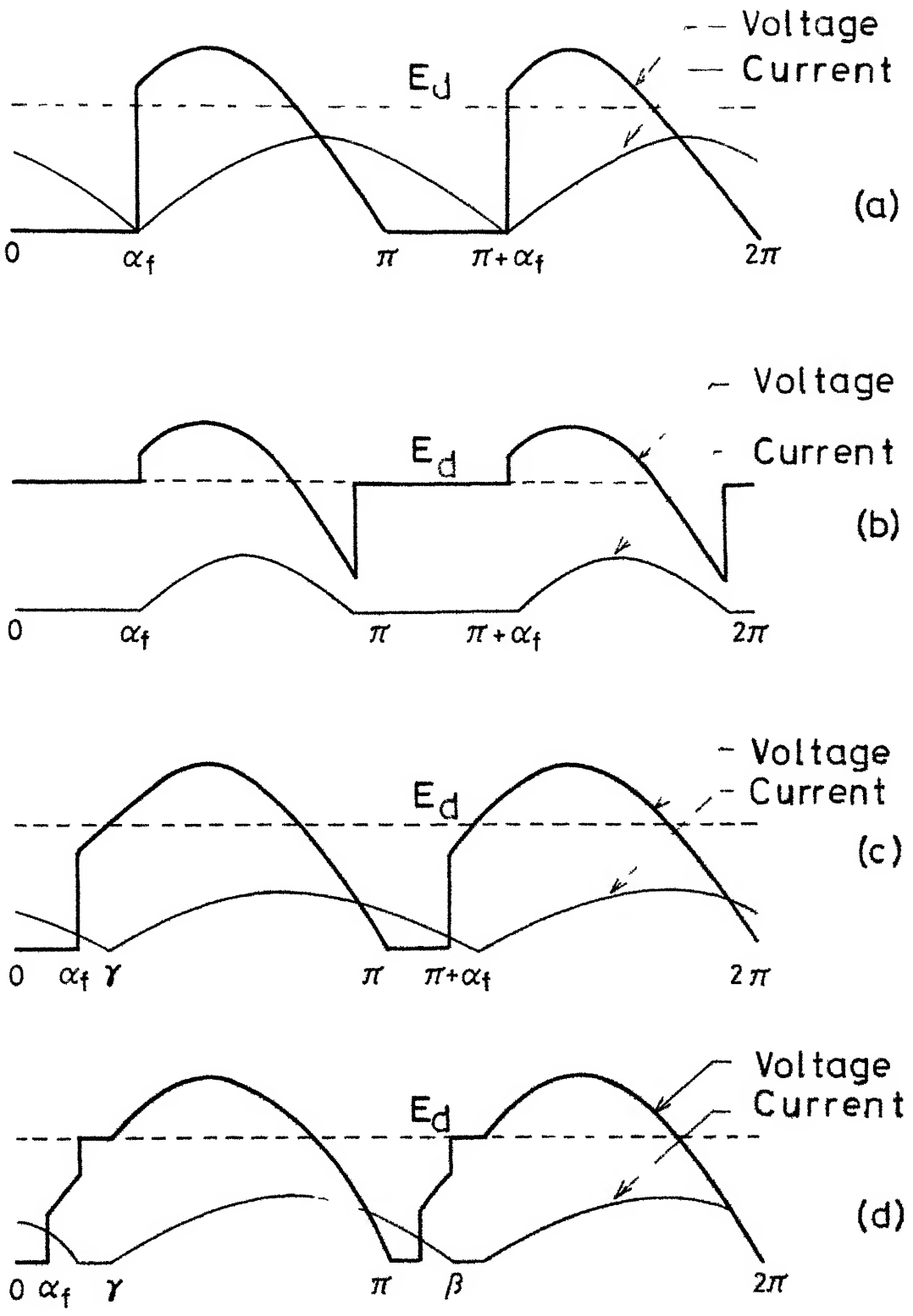

Fig.3-2 Voltage and current waveforms for half controlled operation

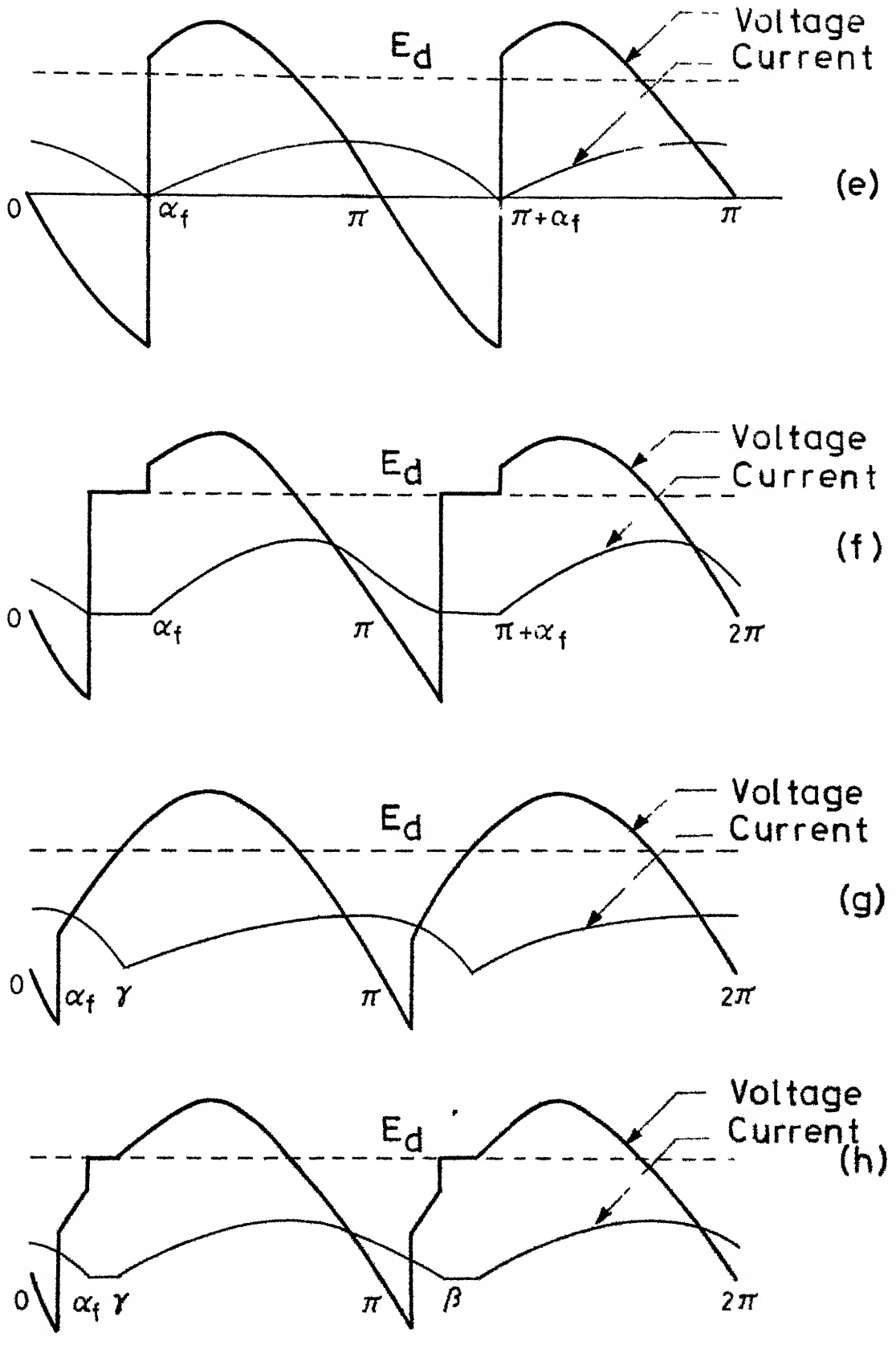

Fig.3·2 Voltage and current waveforms for fully controlled operation

Mode 2 In this mode (Figs 3.2d, 3 2 h), the firing is done at an angle less than γ. The motor back emf being larger than the instantaneous input voltage, the armature current reduces and becomes zero This mode of operation is shown in Figs 3 2d, 3 2h. . It is necessary that the thyristor firing circuit should provide a string of pulses. If the current is continuous, thyristors could be triggered at any point of the input voltage waveform as the motor back emf cannot appear as a reverse bias across the thyristors. The system equations for different intervals will be as follows

3.2a. Fully Controlled Operation

(1) Mode 1 The equivalent circuit is shown in Fig. 3 3(a) The equation governing the system is

$$L_a \frac{di_a}{dt} + R_a i_a + E_d = bE_m \sin\omega t \qquad (3.1)$$

where $b = 1, \quad \alpha_f \leq \omega t \leq \beta \quad (\text{if } \beta < \pi)$

Assuming the initial condition to be zero owing to discontinuity, the solution of (3.1) yields

$$i_a(\omega t) = I_m [\sin(\omega t - \psi) - \sin(\alpha_f - \psi)\exp\{-\cot\psi(\omega t - \alpha_f)\}] - I [1-\exp\{-\cot\psi (\omega t - \alpha_f)\}] \qquad (3.2)$$

Taking the base value of i as $2E_m/\pi R_a$, normalized eqn (3.2) is given by (3.3)

$$i_p(\omega t) = \frac{\pi}{2} \cos\psi [\sin(\omega t - \psi) - \sin(\alpha_f - \psi)\exp\{-\cot\psi(\omega t - \alpha_f)\}] - WN[1-\exp\{-\cot\psi(\omega t - \alpha_f)\}] \qquad (3.3)$$

(ii) Mode 2 When firing angle α_f is less than γ, Mode 2 occurs. Assuming the initial condition to be zero,

$$i_p(\omega t) = \frac{\pi}{2} \cos\psi [\sin(\omega t-\psi) - \sin(\gamma-\psi) \exp\{-\cot\psi(\omega t-\gamma)\}] - WN [1-\exp\{-\cot\psi(\omega t-\gamma)\}], \quad \gamma \leq \omega t \leq \pi+\alpha_f \qquad (3.4)$$

If $\beta \geq \pi + \alpha_f$, $b = -1$ for $\pi + \alpha_f \leq \omega t \leq \beta$ (if $\beta \leq \pi + \gamma$)

$$i_p(\omega t) = \frac{\pi}{2} \cos\psi [-2\sin(\alpha_f-\psi)\exp\{-\cot\psi(\omega t-\pi-\alpha_f)\} - \sin(\gamma-\psi)\exp\{-\cot\psi(\omega t-\gamma)\} - \sin(\omega t-\psi)] - WN [1-\exp\{-\cot\psi(\omega t-\gamma)\}] \qquad (3.5)$$

3.2b. Half Controlled Operation

(i) Mode 1 The dynamics is described by eqn.(3.1) where

$$b = 1 \text{ for } \alpha_f \leq \omega t \leq \pi$$
$$b = 0 \text{ for } \pi \leq \omega t \leq \beta \quad (\text{if } \pi \leq \beta \leq \pi + \alpha_f) \qquad (3.6)$$

Eqn.(3.3) is the solution of (3.6) when b = 1 and (3.7) is the solution of (3.6) when b = 0

$$i_p(\omega t) = \frac{\pi}{2} \cos\psi [\sin\psi \exp\{-\cot\psi(\omega t-\pi)\} - \sin(\alpha_f-\psi)\exp\{-\cot\psi(\omega t-\alpha_f)\}] - WN [1-\exp\{-\cot\psi(\omega t-\alpha_f)\}], \quad \pi \leq \omega t \leq \pi + \alpha_f \qquad (3.7)$$

$$WN = \frac{\pi}{2} \frac{(1+\cos\alpha_f)}{(\beta-\alpha_f)} - TN \frac{\pi}{(\beta-\alpha_f)} \qquad (3.8)$$

(ii) Mode 2 The dynamics is described by eqn.(3.1) where

$$b = 1 \quad \gamma \leq \omega t \leq \pi$$
$$b = 0 \quad \pi \leq \omega t \leq \pi + \alpha_f \qquad (3.9)$$
$$b = -1 \quad \pi + \alpha_f \leq \omega t \leq \beta \quad (\text{if } \pi + \alpha_f \leq \beta \leq \pi + \gamma)$$

Eqn (3 4) is the solution of (3 1) when b = 1 and (3.7) is the solution of (3 1) when b = 0 and (3 10) is the solution of (3 1) when b = -1.

$$i_p(\omega t) = \frac{\pi}{2} \mathrm{Cos}\psi[\mathrm{Sin}\psi \exp\{-\mathrm{Cot}\psi(\omega t-\pi)\} - \mathrm{Sin}(\alpha_f-\psi)\exp\{-\mathrm{Cot}\psi(\omega t-\pi-\alpha_f)\} - \mathrm{Sin}(\gamma-\psi)\exp\{-\mathrm{Cot}\psi(\omega t-\gamma)\} - \mathrm{Sin}(\omega t-\psi)] - WN\,[1-\exp\{-\mathrm{Cot}\psi(\omega t-\nu)\}] \quad \pi+\alpha_f \leq \omega t \leq \pi+\gamma \tag{3 10}$$

$$WN = \frac{\pi}{2} \frac{(1+\mathrm{Cos}\gamma+\mathrm{Cos}\beta+\mathrm{Cos}\,\alpha_f)}{(\beta-\gamma)} - TN \frac{\pi}{(\beta-\gamma)} \tag{3.11}$$

3 2c. Continuous Mode

When the current is continuous, calculations are straightforward The expressions for WN for one quadrant and two-quadrant drives are

$$WN = 0.5(1+\mathrm{Cos}\,\alpha_f) - TN \quad \text{for one-quad drive} \tag{3 12}$$

$$WN = \mathrm{Cos}\,\alpha_f - TN \quad \text{for two-quad drive} \tag{3 13}$$

For a given firing angle, the critical speed WN_c representing the boundary between continuous and discontinuous conduction modes is obtained by letting the conduction period to be π. The expressions are derived as shown below. At this critical speed, the critical torque is also calculated, below which discontinuous conduction takes place.

3.3a. Fully Controlled Operation - Mode 1 :

$$WN = -\frac{\pi}{2}\mathrm{Cos}\psi[\mathrm{Sin}(\alpha_f-\psi)+\mathrm{Sin}(\alpha_f-\psi)\exp\{-\pi\mathrm{Cot}\psi\}]/[1-\exp\{-\pi\mathrm{Cot}\psi\}] \tag{3.14}$$

$$TN = \mathrm{Cos}\,\alpha_f - WN \tag{3.15}$$

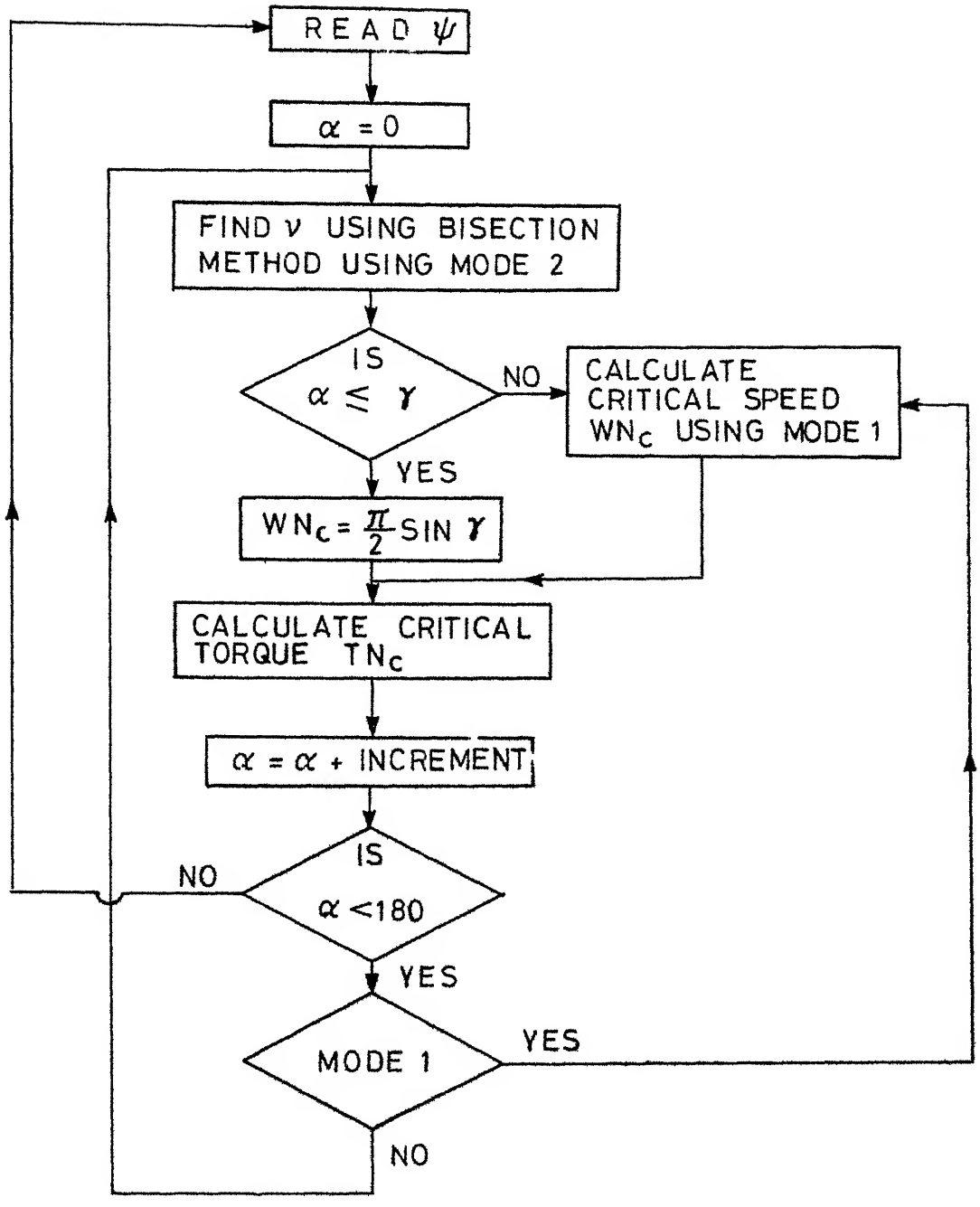

Fig. 3·4 Flow chart for calculating boundaries of Fig. 3·5

3.3b Fully Controlled Operation - Mode 2

$$\frac{\pi}{2}\cos\psi[-2\sin(\alpha_f-\psi)\ \exp\{-\cot\psi(\gamma-\alpha_f)\}\ -\sin(\gamma-\psi)\exp\{-\pi\cot\psi\}$$

$$+\ \sin(\gamma-\psi)]-\ WN[\ 1-\exp\{-\pi\cot\psi\}]\ =\ 0 \qquad (3.16)$$

Critical torque can be calculated using (3 15).

3.4a Half Controlled Operation - Mode 1

$$WN_c = \frac{\frac{\pi}{2}\cos\psi[\sin\psi\exp\{-\cot\psi\ \alpha_f\}\ -\sin(\alpha_f-\psi)\exp\{-\cot\psi\ \pi\}]}{[1\ -\ \exp\{-\cot\psi\ \pi\}]} \qquad (3.17)$$

$$TN_c = 0\ 5(1 + \cos\alpha_f) - WN_c \qquad (3\ 18)$$

3.4b. Half Controlled Operation - Mode 2

$$\frac{\pi}{2}\cos\psi[\sin\psi\exp\{-\cot\psi\gamma\} - \sin(\alpha_f-\psi)\exp\{-(\gamma-\alpha_f)\cot\psi\}$$

$$-\sin(\gamma-\psi)\ \exp\{-\pi\cot\psi\}+\ \sin(\gamma-\psi)\ ]-\ WN\ 1-\exp\{-\pi\cot\psi\}\ ]=\ 0 \qquad (3.19)$$

Critical torque can be calculated using (3.18).

Ripple factor is calculated as in (3.20).

$$RF = (I_{a\,max} - I_{a\,min})/2I_{av} \qquad (3.20)$$

A set of boundaries (Fig 3.5) for various values of ψ are computed as shown in the flow chart (Fig.3.4). Area to the left of the boundary gives discontinuous conduction. A set of maximum value of ripple factor RF versus ψ for various values of speed are also plotted taking continuous conduction into consideration (Fig.3.6). These can be used to choose an optimum value of inductance for a motor as follows.

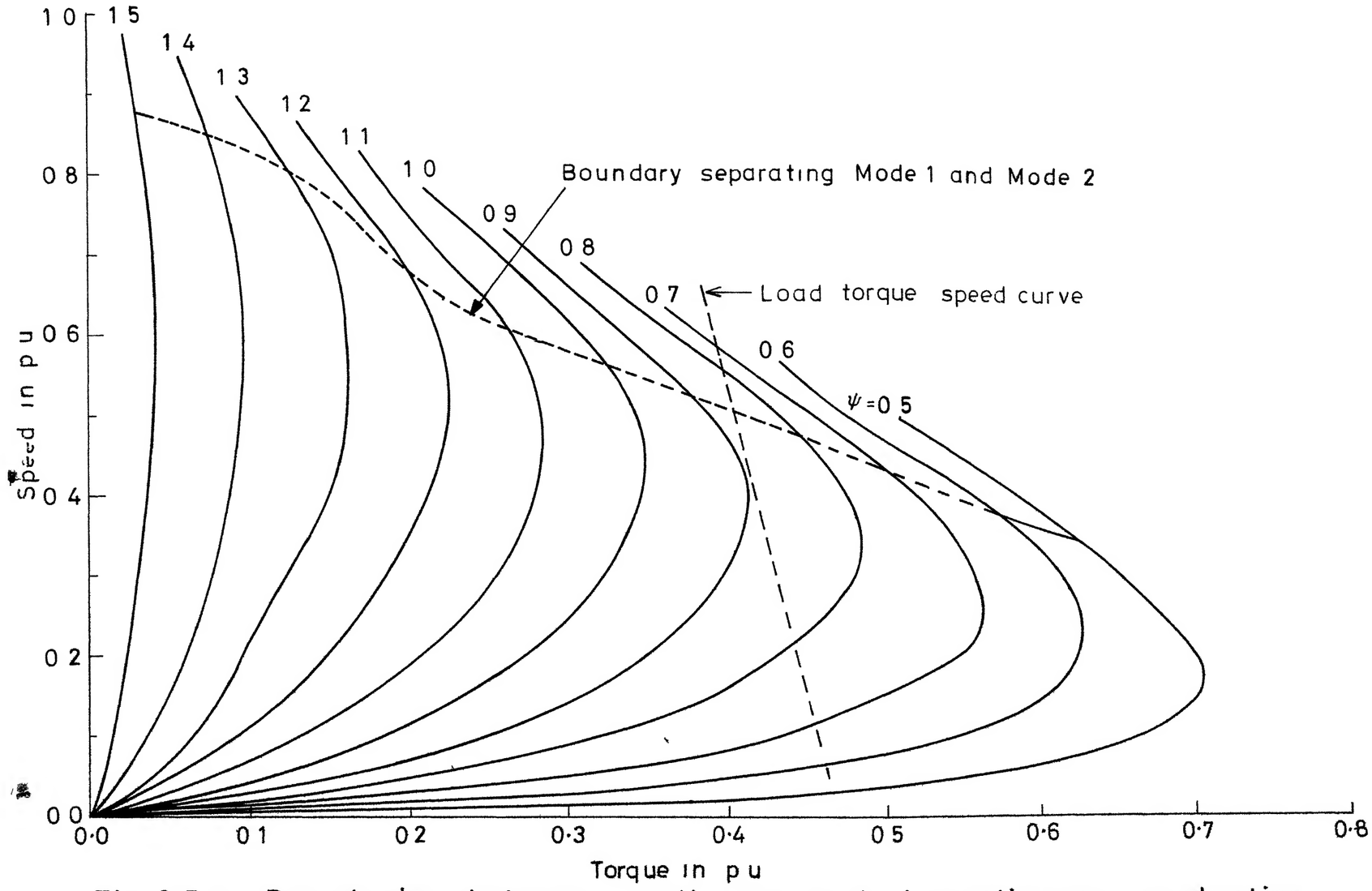

Fig 3·5 a. Boundaries between continuous and discontinuous conduction for half controlled operations

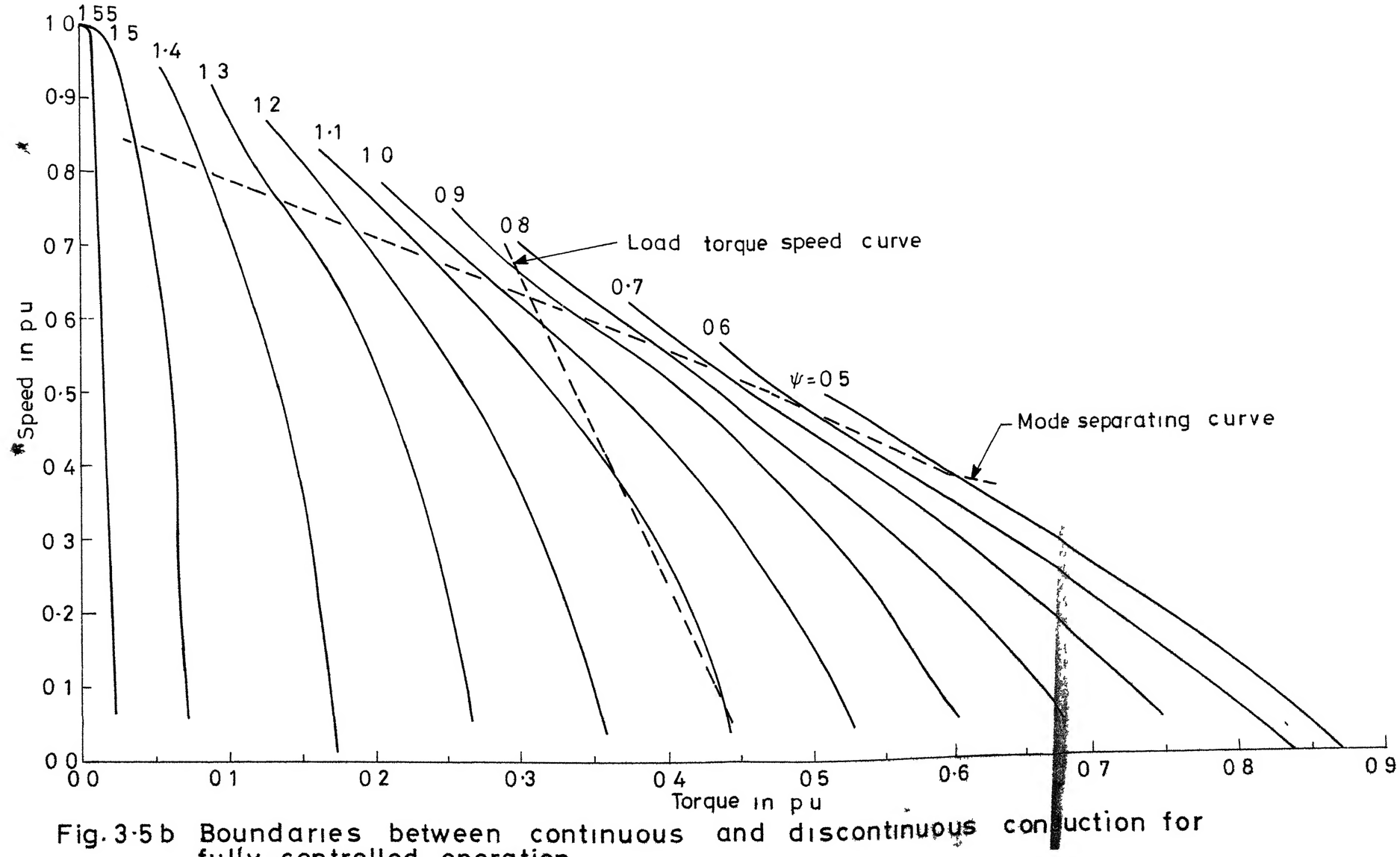

Fig. 3·5 b Boundaries between continuous and discontinuous conduction for fully controlled operation

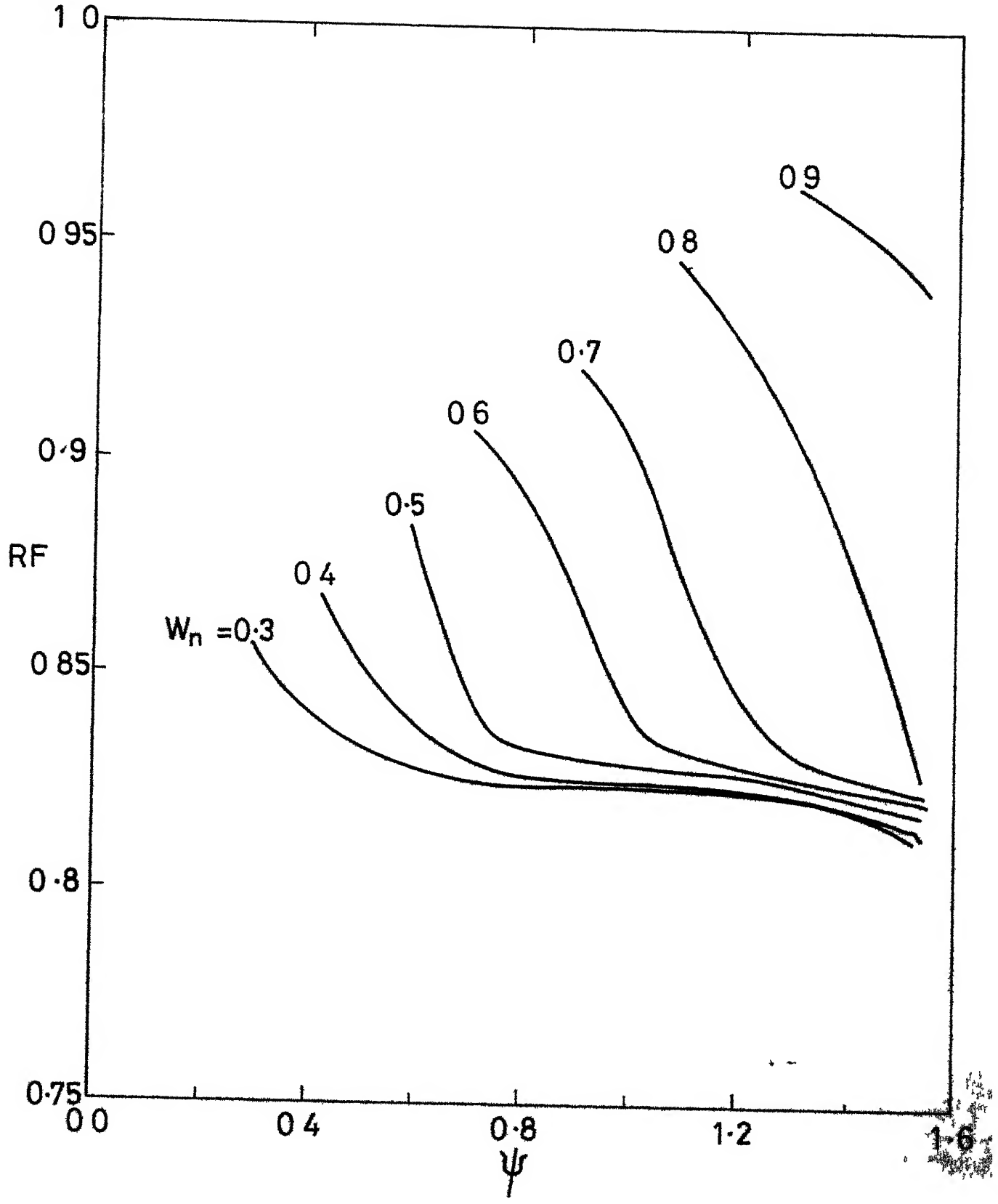

Fig. 3·6 a. Half controlled characteristics

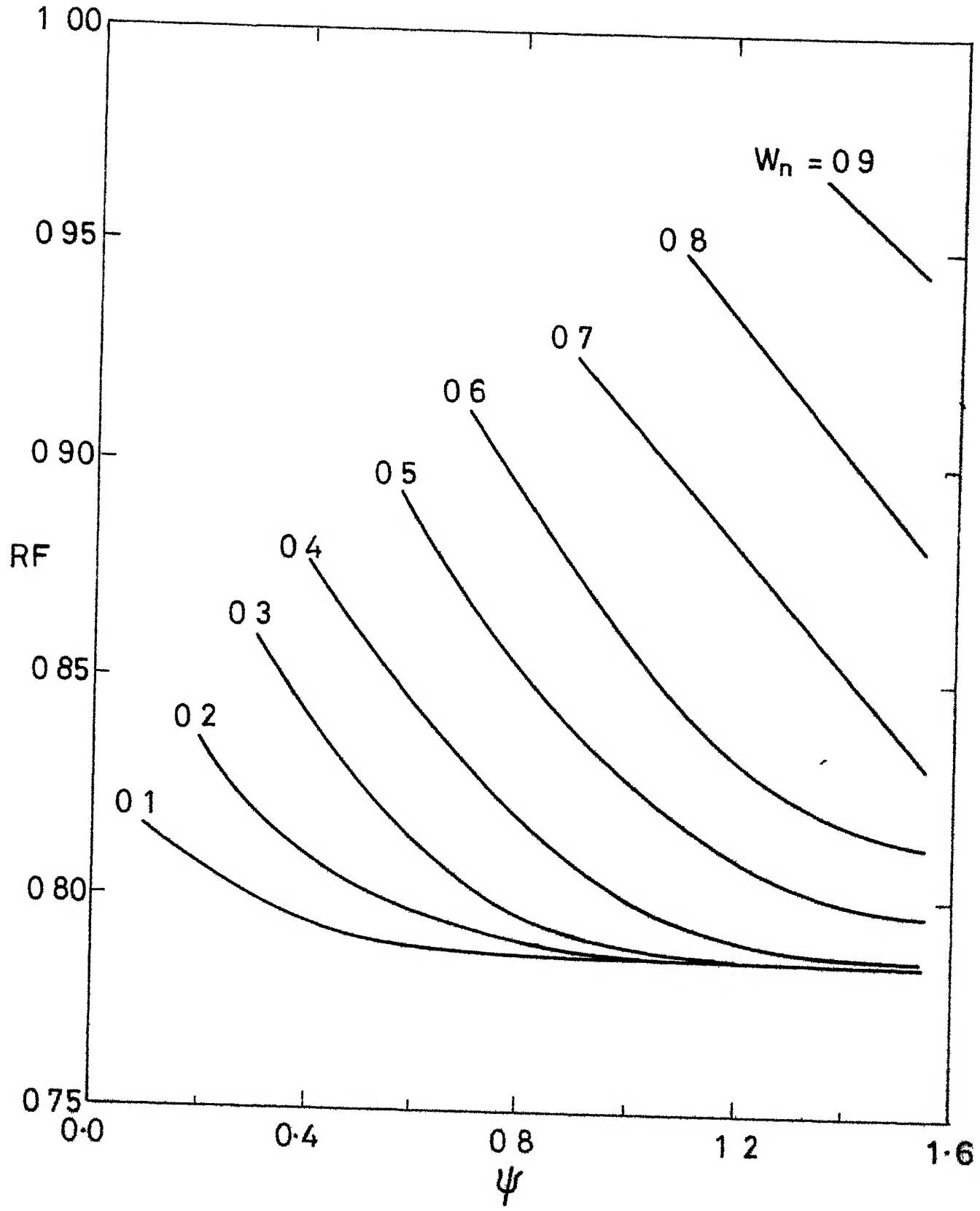

Fig.3·6b. Fully controlled characteristics

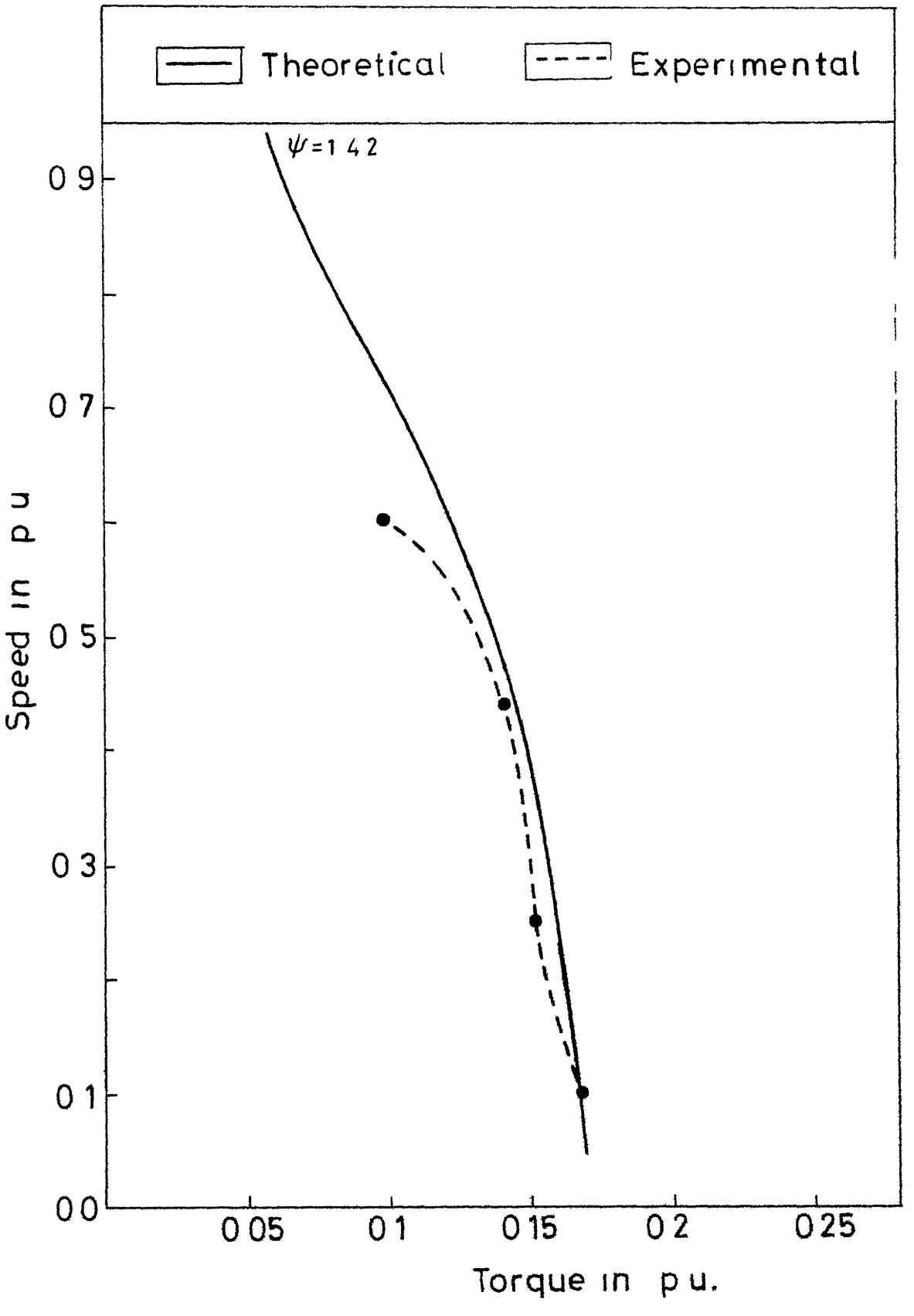

Fig. 3 7 Experimental verification of Fig 3·5

3.5 CHOICE OF FILTER INDUCTANCE

Minimum values of developed torque for various speeds are obtained from the requirement of the load being driven by the motor. If the motor is expected to operate under no-load, the minimum torque denoted will be due to coulomb and viscous friction only. Normalized values of these are plotted in Fig. 3.5 as shown by dotted lines For discontinuous conduction to be absent, values of ψ should be such that the boundary separating continuous and discontinuous conduction lies to the left of this curve. After ψ is chosen, one can check using Fig 3.6 whether the maximum value of ripple is within permissible value or not at the critical operating speed. If it is not, one should try the larger value of ψ .

3.6 EXPERIMENTAL VERIFICATION

The boundary between continuous and discontinuous conduction for a value of $\psi = 1.42$ is verified experimentally. As the firing angle is varied, critical torque and critical speed are measured at which just continuous conduction takes place The curve which separates the continuous and discontinuous conduction regions is shown in Fig. 3.7 with dotted lines. The continuous line shows the theoretically computed characteristic

CHAPTER IV

SYSTEM ORGANIZATION

4.1 INTRODUCTION

Closed loop controlled dc drives are widely used because of versatile control characteristics of the dc separately excited motor. The converter controlled dc drive known as static ward Leonard scheme is fast replacing the conventional ward Leonard drive. Basic scheme of a speed control system employing current limit control is shown in Fig. 4.1.

In this scheme V_{ref} sets the speed reference. Speed sensor output after filtering is compared with reference speed setting and the speed error signal is fed to speed controller. Speed controller tries to make the system steady state speed error zero DC current sensor measures the motor armature current. If the motor current is less than I_x, current controller does not affect the performance of the motor However, if I_a exceeds I_x even by a small amount, large output voltage is developed by current controller. The speed control goes out of action and the speed is adjusted according to the permitted current As soon as the current falls below I_x, current controller output again becomes zero and speed controller takes over the operation.

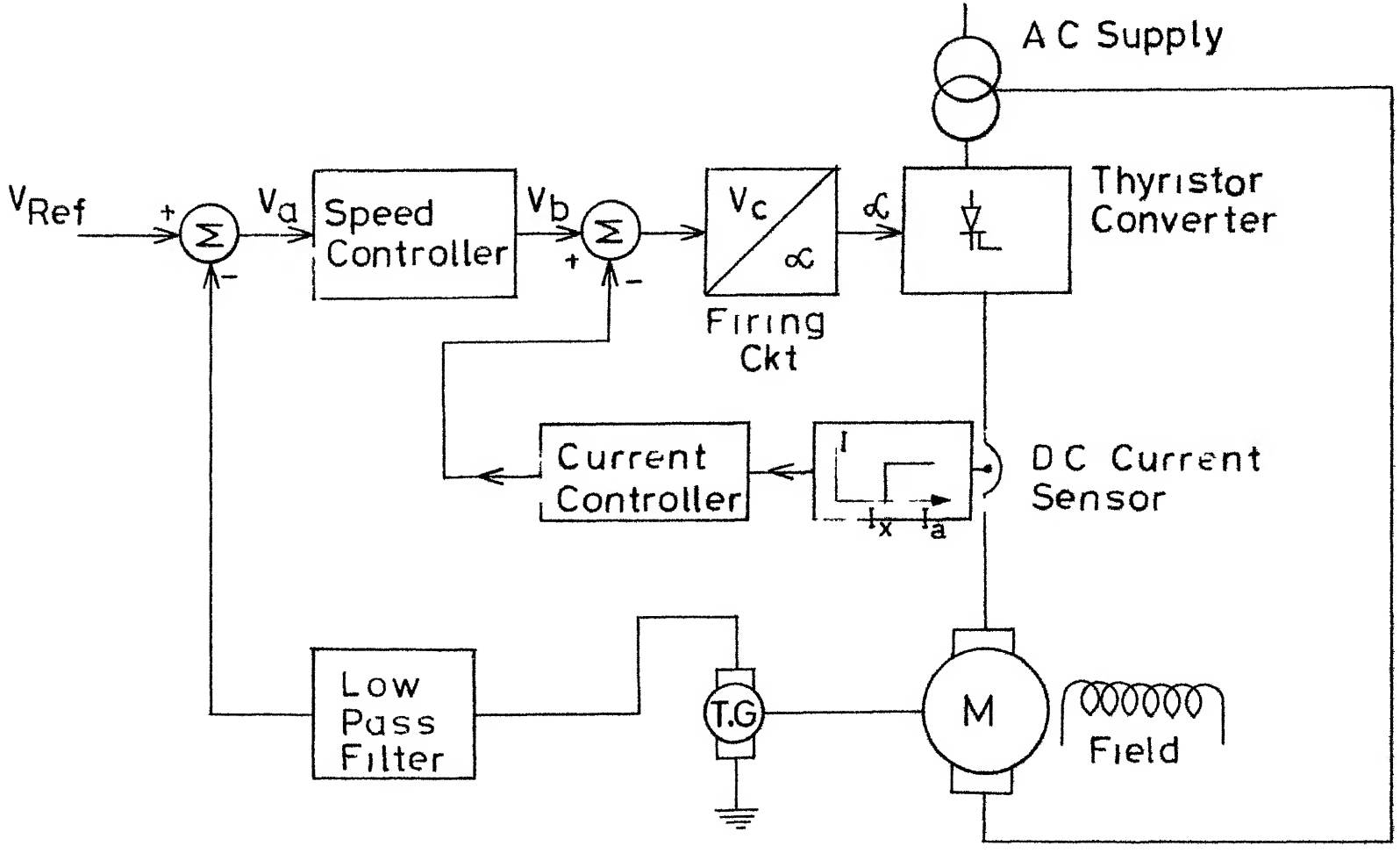

Fig 4.1 Basic scheme of speed control system with current limit control

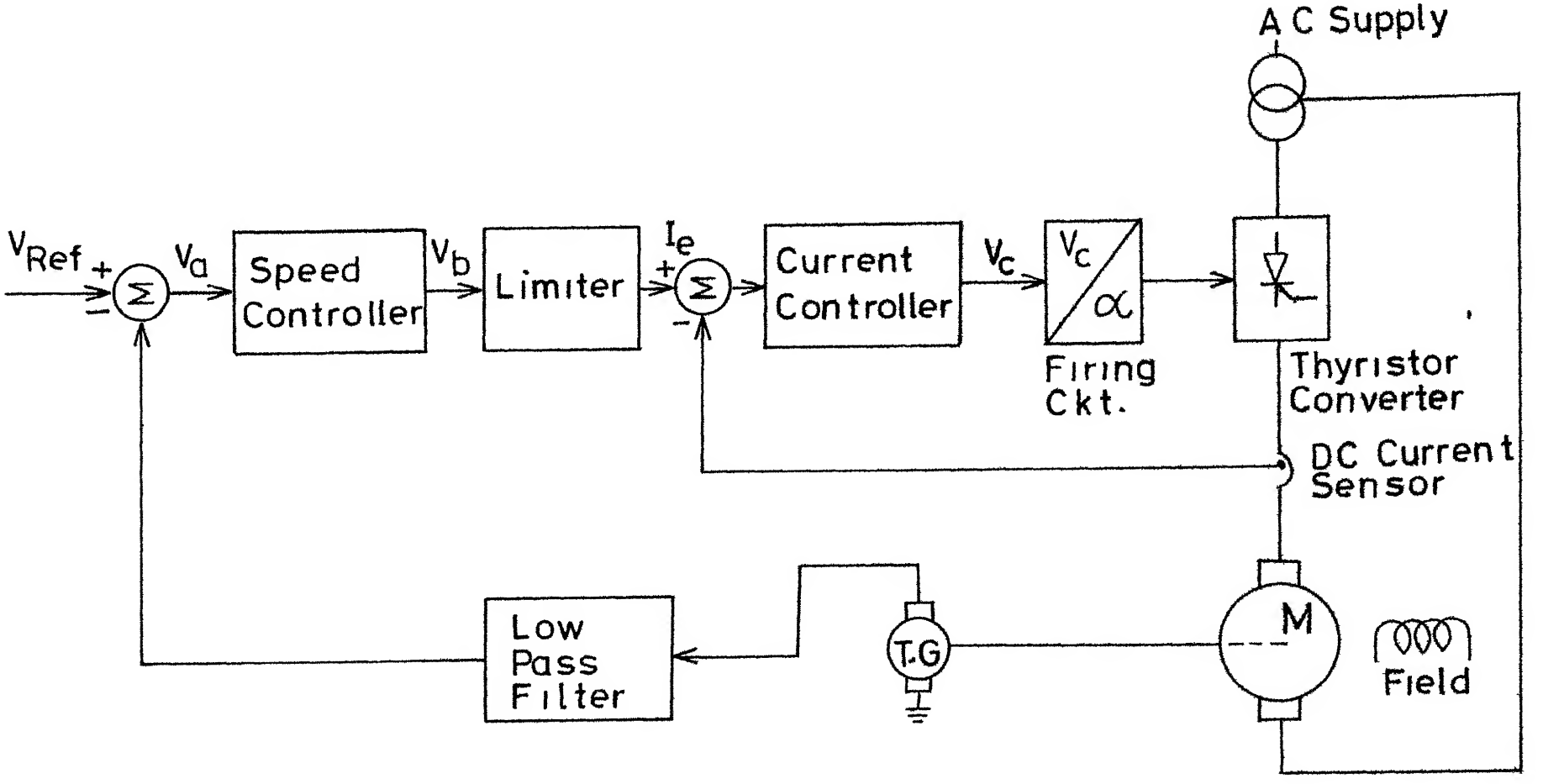

Fig. 4·2 Schematic diagram of speed control system with inner current control loop

Another scheme of speed control system employing inner current control loop which is in cascade with the speed control is shown in Fig 4 2. Here the output magnitude of the speed controller is the desired value for the current control circuit. When there is a drop in speed, the speed difference which passes through the speed controller produces a higher desired current value and thus the speed difference is corrected The desired current value can be adjusted to higher values to keep the speed at the desired value, as long as it does not exceed the value preset by the current limiter The limiter limits the maximum reference value for the current control loop and is so desined that its maximum output corresponds to the maximum permissible current of the converter motor set up. The inner current control loop scheme of Fig.4.2 has the following advantages over the scheme shown in Fi 4.1.

While starting, if the firing angle is reduced to a small value in absence of current control, starting current may shoot up to a large value and damage the thyristors. Similarly overloads and load disturbances may cause the current to exceed safe values. The current loop does not permit large values of current to flow. The inner current loop also provides fast response against the supply disturbances. Since the electrical time constant of the motor armature is small compared to the mechanical time constant,

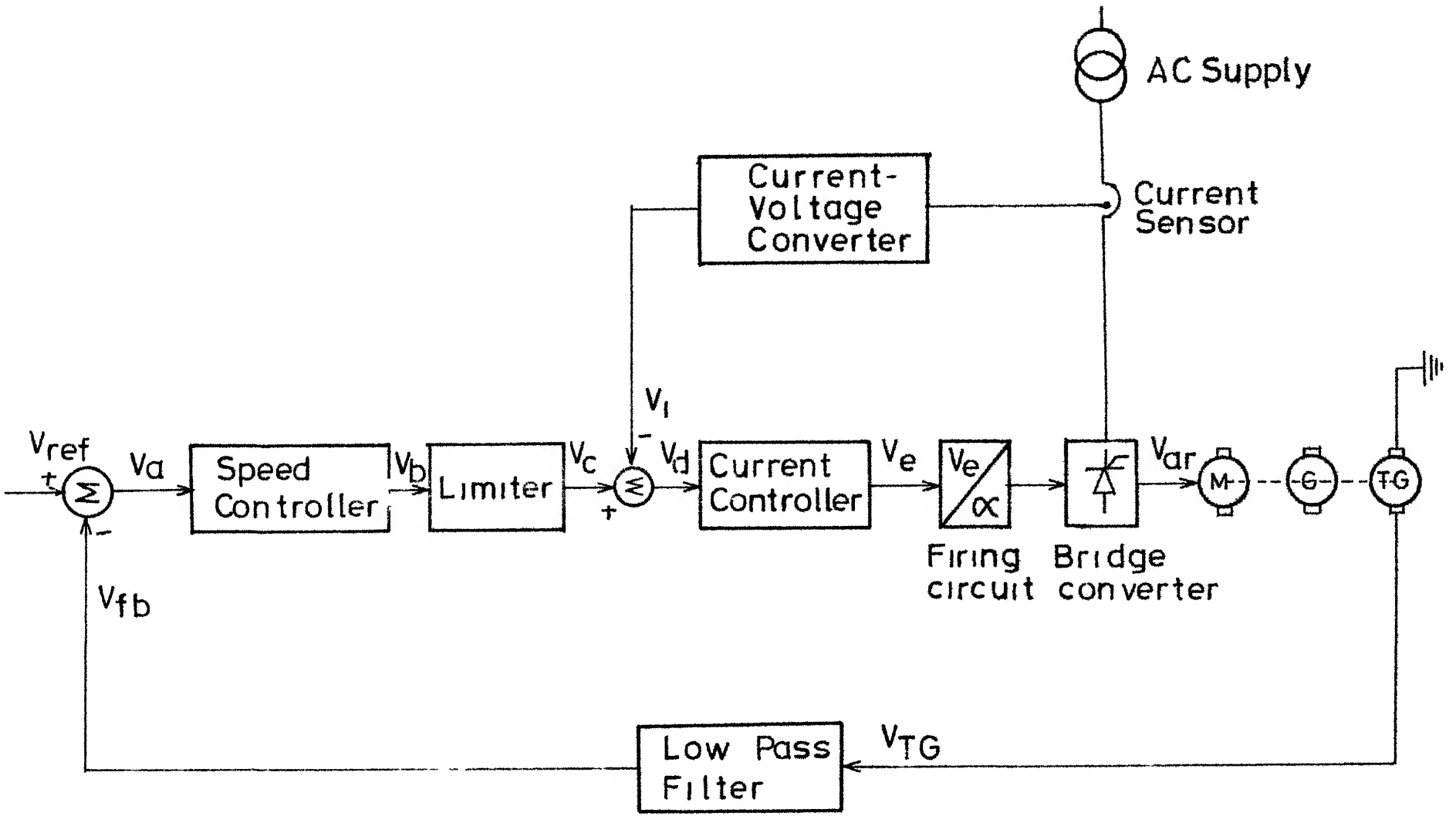

Fig 4 3 Schematic diagram of motor speed control system controlled by thyristor converter

the armature current rather than the speed drops almost instantaneously whenever the supply voltage falls. In the absence of the inner current control loop, the motor decelerates to cope with the load torque The speed comes back to the original value after the drop in speed is processed by the speed controller to give a new firing angle. Hence for corrective action to take place, a change in speed has to accompany a change in the supply voltage and the response is poor owing to the large mechanical time constant involved. With the inner current control loop present, a drop in armature current itself results in a new firing angle and the fall in supply voltage is counteracted by correcting the armature current at a fast rate

4 2 REALISATION OF THE SYSTEM

The scheme that has been used is shown in Fig. 4.3. and the various blocks and their technical details are discussed below

Speed Sensor

In general two methods are used for speed sensing. In one of the methods, induced voltage is sensed by sensing the motor terminal voltage and armature resistance drop and obtaining the difference of the two. But the signal is directly affected by the deviations of the field flux under saturation and line voltage changes, and by temperature linearity and setting of the armature voltage circuit. Though

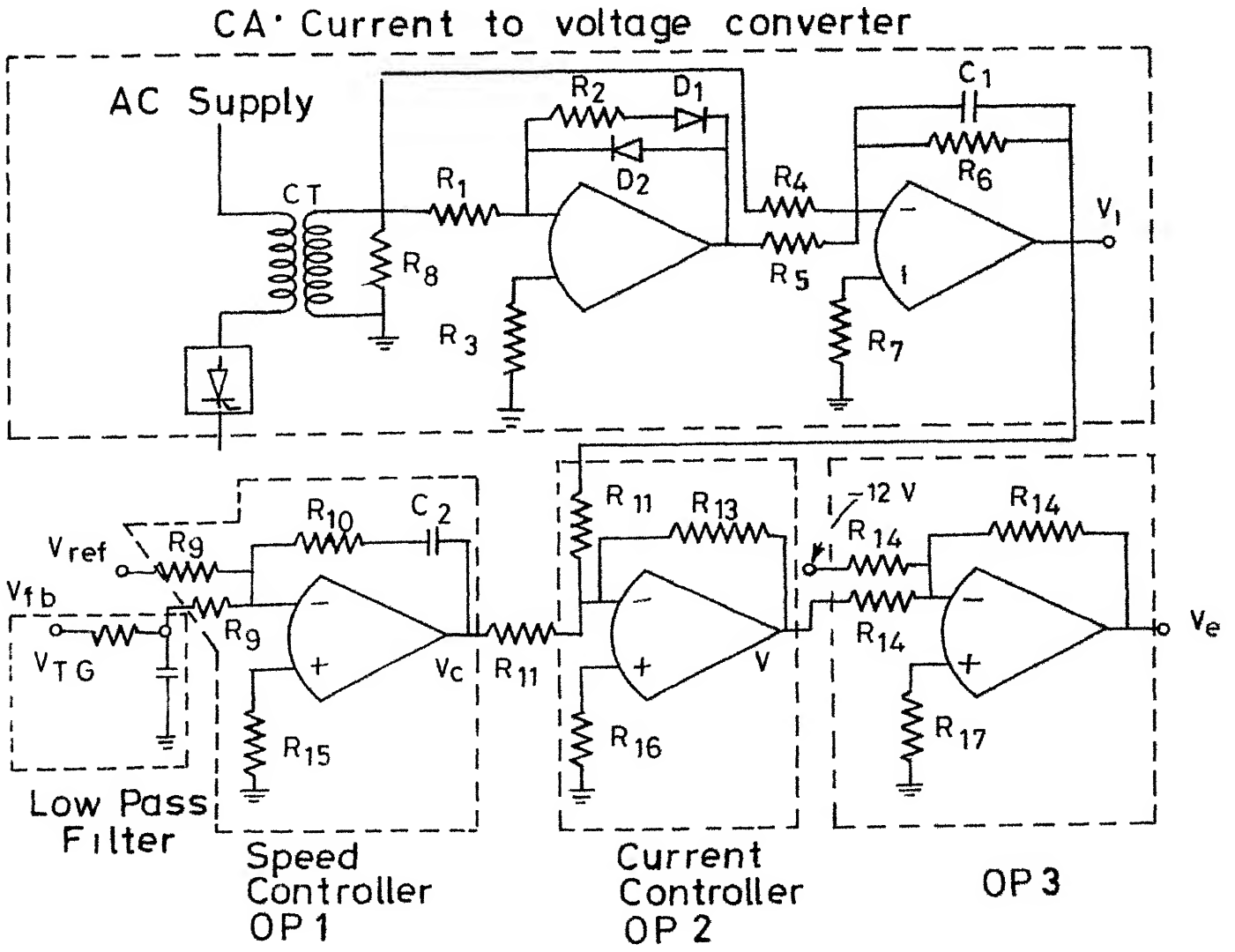

Fig. 4·4 Control circuit of motor speed control system

the method is practical and inexpensive, more accurate speed regulation is achieved by using a tachogenerator driven from the motor shaft The tachogenerator is a dc generator which has a higher order of linearity between its speed and output voltage. The commutator of the tachogenerator produces ripple on the output voltage. The ripple is filtered out by a low pass filter whose break frequency does not fall into the control loop range and affect the dynamics of the system. This is realised by F_1 in Fig 4.4.

Current Sensing

A signal proportional to the armature current is required for ~~one~~ the current control loop. The techniques that are used for current sensing are 1. shunt resistance in the armature circuit 2. dc transductor or Hall Effect Current probe in the armature circuit 3. Current transformer in the ac line.

To make the system inexpensive and to isolate the control circuit from the power circuit current,transformer in the ac line has been used. A small resistance is connected across the secondary terminals of the current transformer and the voltage across the secondary terminals is rectified to yield a signal proportional to armature current. A bridge rectifier has been used in the literature [16]. Since the voltage to be rectified is of low level because of very small resistance connected across the secondary terminals

of current transformer, Op-Amp ac to dc converters has been used. The reasons are as follows. Although semiconductor diodes are close to ideal diodes, they have severe limitations in low voltage level applications. Silicon diodes have 0 6V threshold which must be overcome before appreciable conduction occurs By placing a diode in the feedback loop of an operational amplifier, the threshold voltage is divided by the open loop gain of an operational amplifier. With the threshold virtually eliminated, it is possible to rectify millivolt signals The circuit that has been used is shown by the block CA in Fig.4 4

Speed Controller and Limiter

There are two types of electronic controllers. 1 Proportional controller 2 Proportional integral controller (called P-I). Proportional controller gives appreciable steady state error whereas P-I type gives nearly zero steady state error. The P-I controller is used in the present scheme which is realised by OP-1 of Fig 4.4 This also acts as a limiter of Fig 4 3.

Current Controller

A proportional controller is used for the current controller. It is realised by OP-2 as shown in Fig 4.4.

Firing Circuit

Firing circuit is discussed in Chapter 2. The relationship between the control voltage V_e and firing angle α_f is

given by $\alpha_f = \pi(1 - V_e/V_m)$ where V_m is the maximum control voltage It is realised by OP-3 in Fig 4.4.

4.3 SYSTEM MODELLING

The transfer functions of the various blocks are derived as shown below

Transfer Functions of Various Elements

DC Motor The differential equations governing the operation of the dc motor are as follows

$$\frac{L_a \, di_a}{dt} + R_a i_a + K_v \omega = V_a(t) \qquad (4.1)$$

$$J \frac{d\omega}{dt} + B\omega + T_l = K_t \, i_a(t) \qquad (4.2)$$

The viscous friction torque has been assumed to be a linear function of speed. Coulomb and static friction are neglected to make the motor model linear. These assumptions are justifiable in the speed control situation as stiction phenomenon is not present while running and Coulomb friction is very small. A block diagram representation of the motor is given in Fig 4 5a

Thyristor Converter The thyristor converter characteristic under continuous conduction shown in Fig. 4.5b. This is a cosine curve in which the average voltage across the output terminals is plotted against the firing angle. Thus

$$V_a = \frac{2E_m}{\pi} \cos \alpha_f \qquad (4.3)$$

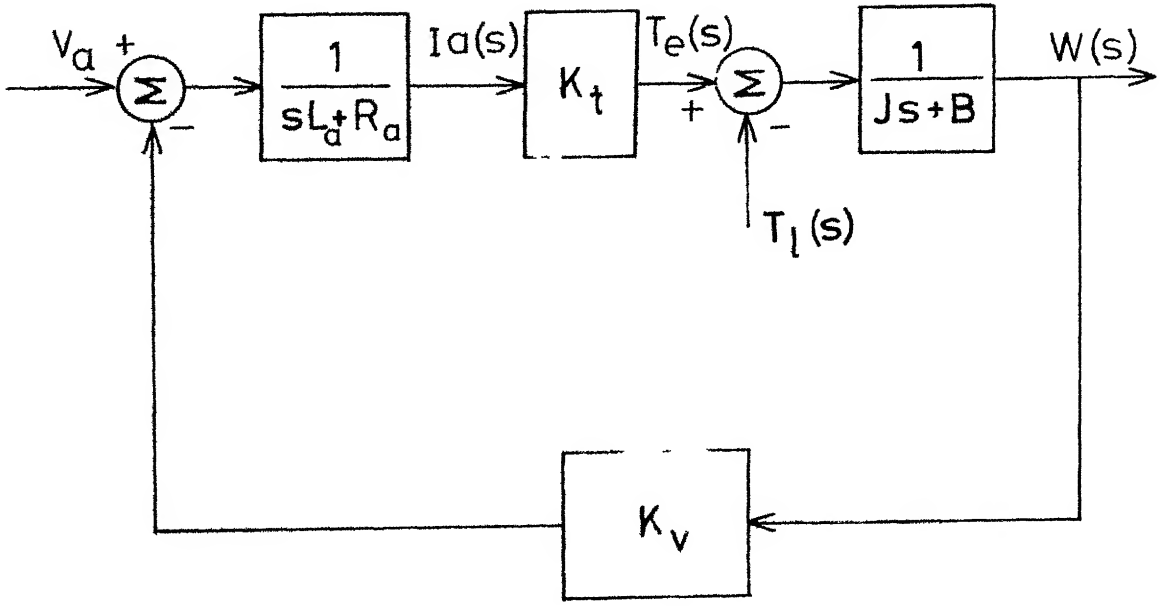

Fig.4·5a. Block diagram of a DC motor

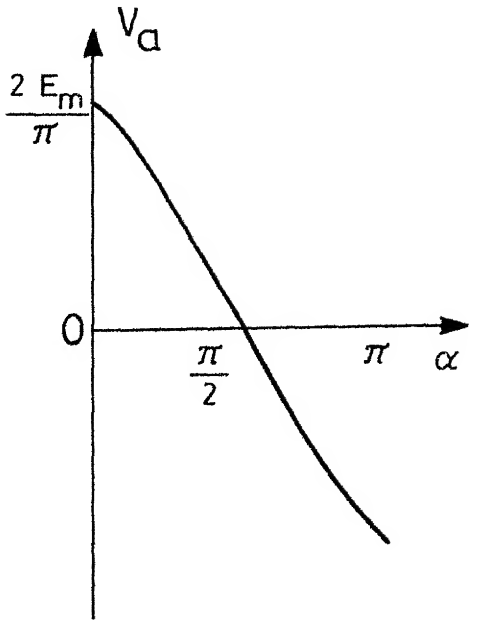

Fig 4 5b. Characteristic of a converter

The firing circuit is designed and adjusted such that the firing angle varies linearly with V_d

$$\alpha_f = \pi \left(1 - \frac{V_d}{V_m}\right) \qquad (4.4)$$

Although the firing angle α_f is proportional to V_d, the firing of the bridge is not instantaneously corrected Once the firing pulse occurs, the information in V_d is of no value until the next firing occurs. Hence any system using a thyristor power amplifier should be regarded as a sample data system in a strict sense To make the analysis simpler it can be approximated as a high gain amplifier [16].

Current Controller A proportional amplifier has been used as current controller Its transfer function is represented by pure gain K.

Current Transducer The block CA in Fig.4.4 is designed such that the voltage V_1 is proportional to current i_a The gain of this system is

$$K_{f1} = V_1/i_a \text{ Volts/ amp.} \qquad (4.5a)$$

Speed Controller and Speed Transducer A P-I controller has been chosen for speed control. The transfer function of the controller is $K_{s1}(1 + s\,\tau_a)/s\,\tau_a$. The tachogenerator gives an output voltage proportional to speed. The transfer function of the tachogenerator is approximated as K_{fs} neglecting the time constant of the low pass filter.

$$K_{fs} = V_{fb}/\omega \quad \text{Volts/rad/sec.} \tag{4 5b}$$

The complete system block diagram is shown in Fig. 4 6

The block diagram shown in Fig 4.6 yields the following system equations

$$\frac{di_a}{dt} = -\frac{R_a}{L_a} i_a - \frac{K_v}{L_a}\omega + \frac{2E_m}{\pi L_a}\cos\alpha_f \tag{4 6}$$

$$\frac{d\omega}{dt} = \frac{K_t}{J} i_a - \frac{B}{J}\omega - \frac{T_l}{J} \tag{4 7}$$

$$\frac{d}{dt}\alpha_f = X i_a + Y\omega + Z\cos\alpha_f + I_1 \tag{4 8}$$

where

$$X = \frac{K_1\pi}{V_m}\left(\frac{K_{s1} K_{fs} K_t}{J} - K_{f1}\frac{R_a}{L_a}\right) \tag{4 9}$$

$$Y = \frac{K_1\pi}{V_m}\left(K_s F_{fs} - K_{s1} K_{fs}\frac{B}{J} - K_{f1}\frac{K_v}{L_a}\right) \tag{4 10}$$

$$Z = \frac{K_1\pi}{V_m} K_{f1}\frac{2E_m}{\pi L_a} \tag{4.11}$$

$$I_1 = \frac{K_1\pi}{V_m}\left(-K_s V_{ref} - K_{s1} K_{fs}\frac{T_l}{J}\right) \tag{4.12}$$

$K_s - K_{s1}/\tau_a$

The steady state operating point is given by

$$\left.\begin{aligned} \omega_\infty &= V_{ref}/K_{fs} \\ i_{a\infty} &= (T_l + B\omega_\infty)/K_t \\ \alpha_{f\infty} &= \text{ARCos}\left((R_a i_{a\infty} + K_v\omega_\infty)\frac{\pi}{2E_m}\right) \end{aligned}\right\} \tag{4 13}$$

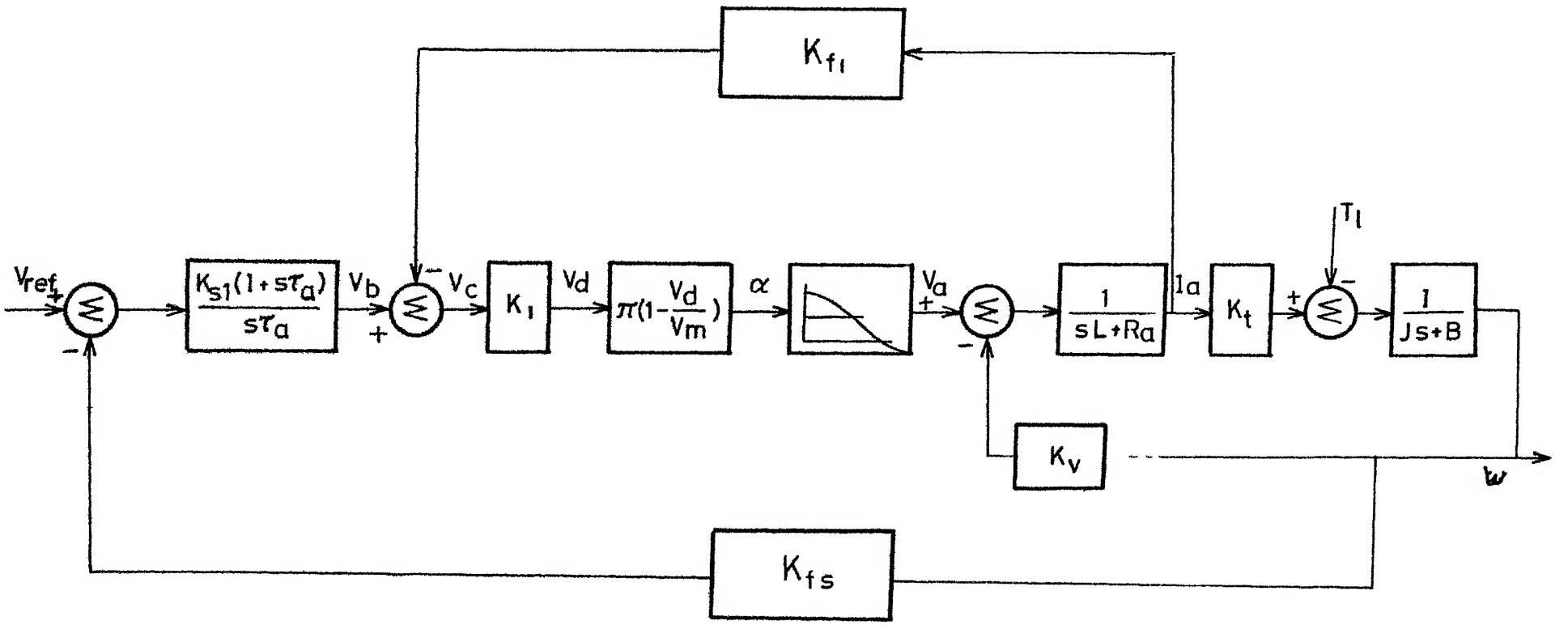

Fig. 4 6 Block diagram of the speed control system

4.4 STABILITY ANALYSIS IN THE SMALL AROUND THE OPERATING POINT

Linearizing the system equations around the operating point, we obtain

$$\frac{d}{dt}\begin{bmatrix} \Delta i_a \\ \Delta\omega \\ \Delta\alpha_f \end{bmatrix} = \begin{bmatrix} -\frac{R_a}{L_a} & -\frac{K_v}{L_a} & -\frac{2E_m}{\pi L_a}\sin\alpha_{f\infty} \\ \frac{K_t}{J} & -\frac{B}{J} & 0 \\ X & Y & -Z\sin\alpha_{f\infty} \end{bmatrix} \begin{bmatrix} \Delta i_a \\ \Delta\omega \\ \Delta\alpha_f \end{bmatrix} \qquad (4.14)$$

The system characteristic equation is

$$\begin{vmatrix} \lambda + \frac{R_a}{L_a} & \frac{K_v}{L_a} & \frac{2E_m}{\pi L_a}\sin\alpha_{f\infty} \\ -\frac{K_t}{J} & \lambda + \frac{B}{J} & 0 \\ -X & -Y & \lambda + Z\sin\alpha_{f\infty} \end{vmatrix} = 0 \qquad (4.15)$$

Simplifying,

$$\lambda^3 + \{\frac{R_a}{L_a} + \frac{B}{J} + Z\sin\alpha_{f\infty}\}\lambda^2 + \{\frac{BR_a}{JL_a} + \frac{K_vK_t}{JL_a} + (\frac{R_a}{L_a} + \frac{B}{J})Z\sin\alpha_{f\infty} + \frac{2E_m}{\pi L_a}X\sin\alpha_{f\infty}\}\lambda + \{(\frac{BR_a}{JL_a} + \frac{K_vK_t}{JL_a})Z\sin\alpha_{f\infty} + \frac{2E_m}{\pi L_a}\sin\alpha_{f\infty}(\frac{K_t}{J}Y + \frac{BX}{J})\} = 0 \qquad (4.16)$$

For the system to be locally stable, the roots of the characteristic equation should lie in the left half-plane.

4.5 DESIGN OF CONTROLLERS

The controllers are designed on the assumption that the system is locally stable. Assume the appropriate eigenvalues λ_i ($i = 1, \ldots, 3$) to ensure local stability. Substituting these eigenvalues in eqn (4.16)

$$\left[\frac{2E_m}{\pi L_a}\sin\alpha_{f\infty}\left(\frac{B}{J}+\lambda_1\right)\right]X+\left[\frac{2E_m}{\pi L_a}\sin\alpha_{f\infty}\frac{K_t}{J}\right]Y$$

$$+\left[\lambda_1^2\sin\alpha_{f\infty}+\left(\frac{R_a}{L_a}+\frac{B}{J}\right)\lambda_1\sin\alpha_{f\infty}+\sin\alpha_{f\infty}\left(\frac{BR_a}{JL_a}+\frac{K_vK_t}{JL_a}\right)\right]Z$$

$$+\left[\lambda_1^3+\left(\frac{R_a}{L_a}+\frac{B}{J}\right)\lambda_1^2+\left(\frac{R_a}{L_a}\frac{B}{J}+\frac{K_vK_t}{JL_a}\right)\lambda_1\right]=0\,,$$

$$(i = 1,\ldots,3) \qquad (4.17)$$

Eqn.(4.17) is solved for X, Y and Z. From (4.9) to (4.11),

$$\left.\begin{aligned}
K_i &= -\frac{V_m}{\pi K_{f1}}\frac{\pi L_a}{2E_m}Z\\
K_{s1} &= -\left(X-\frac{K_i\pi}{V_m}K_{f1}\frac{R_a}{L_a}\right)\frac{V_m}{K_1\pi}\frac{J}{K_tK_{fs}}\\
K_s &= \left(Y+\frac{K_1\pi}{V_m}K_{s1}K_{fs}\frac{B}{J}+\frac{K_i\pi}{V_m}K_{f1}\frac{K_v}{L_a}\right)\frac{V_m}{K_1K_{fs}}
\end{aligned}\right\} \qquad (4.18)$$

$$\tau_a = K_{s1}/K_s.$$

Controllers are designed for the operating point 30°. The values are given in Table 4.1. For the designed values, system stability at all operating points is verified and the results are given in Table 4.2.

4.6 STABILITY ANALYSIS IN THE LARGE

Since the system has been designed assuming that the system is locally stable, stability is to be checked in the large. Popov's criterion has been applied to check the system stability in the large.

Let

$$x_1 = i_a - i_{a\infty}$$

$$x_2 = w - w_\infty \tag{4.19}$$

$$x_3 = \alpha_f - \alpha_{f\infty}$$

Equations (4.6) to (4.8) can be written as

$$\dot{x}_1 = -\frac{R_a}{L_a} x_1 - \frac{K_v}{L_a} x_2 - \frac{2E_m}{\pi L_a}\{\cos \alpha_{f\infty} - \cos(x_3 + \alpha_{f\infty})\}$$

$$\dot{x}_2 = \frac{K_t}{J} x_1 - \frac{B}{J} x_2 \tag{4.20}$$

$$\dot{x}_3 = X x_1 + Y x_2 - Z\{\cos \alpha_{f\infty} - \cos(x_3 + \alpha_{f\infty})\}$$

Or, in vector-matrix notation, as

$$\dot{\underline{x}} = \begin{bmatrix} -\frac{R_a}{L_a} & -\frac{K_v}{L_a} & 0 \\ \frac{K_t}{J} & -\frac{B}{J} & 0 \\ X & Y & 0 \end{bmatrix} \underline{x} + \begin{bmatrix} -\frac{2E_m}{\pi L_a} \\ 0 \\ -Z \end{bmatrix} f(\sigma) \tag{4.21}$$

where

$$\sigma = [\,0 \quad 0 \quad 1\,]\,\underline{x}$$

and

$$f(\sigma) = \text{Cos}\ \alpha_{f\infty} - \text{Cos}(x_3 + \alpha_{f\infty})$$

In the dc drive firing angle varies from 0 to π radians. So the maximum value of α_f, i.e $x_3 + \alpha_{f\infty}$ is π The minimum value of α_f, i e., $x_3 + \alpha_{f\infty}$ is 0 Thus, the constraint to be satisfied by x_3 is

$$-\alpha_f \leq x_3 \leq \pi - \alpha_{f\infty}$$

In order to facilitate the application of Popov's criterion, we will incorporate the constraint on firing angle differently from that given above. It is observed in eqn.(4 21) that the state variable x_3 appears in the right handside only in the nonlinear function f in the second term. Thus, instead of putting a constraint on the state variable x_3, we will define a new nonlinear function $\phi(x_3)$ which will incorporate the firing angle constraint. Thus, let

$$\left.\begin{aligned} \phi(x_3) &= f(x_3 \qquad \text{if } -\alpha_{f\infty} \leq x_3 \leq \pi - \alpha_{f\infty} \\ &= f(-\alpha_{f\infty}) \quad \text{if } x_3 \leq -\alpha_{f\infty} \\ &= f(\pi - \alpha_{f\infty}) \quad \text{if } x_3 > \pi - \alpha_{f\infty} \end{aligned}\right\} \qquad (4.23)$$

It can be checked easily that the nonlinear function lies in the first and third quadrants. It is shown graphically in Fig. 4.7.

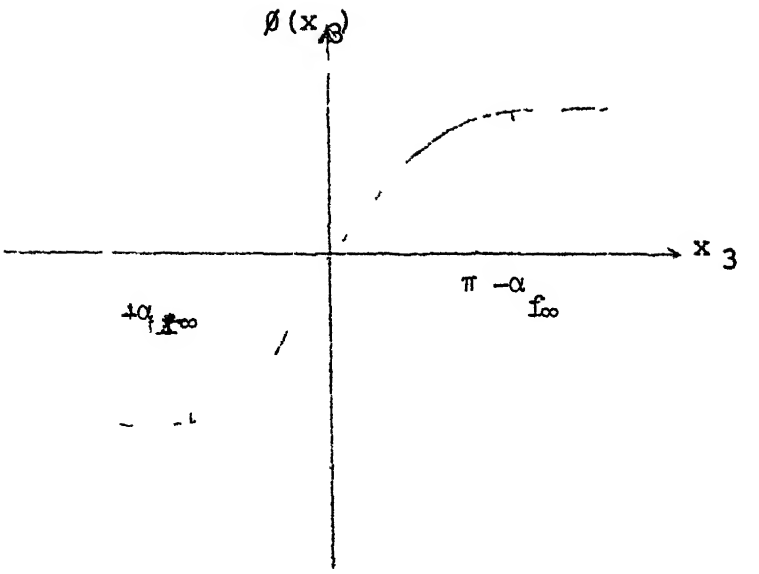

Fig 4.7

Since the nonlinearity lies in the first and third quadrant, Popov's frequency condition can be applied (Appendix B). For this purpose the system is represented as shown in Fig. 4 8a

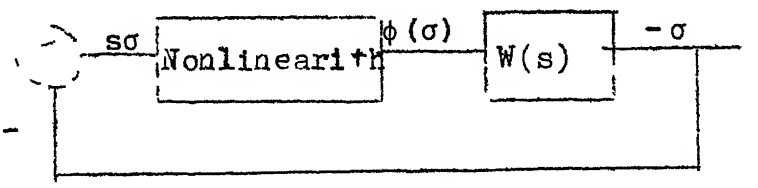

Fig. 4.8a

The transfer function W(s) is

$$W(s) = -\frac{x_3(s)}{\phi_\sigma(s)}$$

$$= \frac{\frac{2E_m}{\pi}[\,J\,X\,s + (B\,X + Y\,K_t + Z_1)\,]}{s[\,(sL_a+R_a)(J\,s + B)+(\,K_v\,K_t)]} \qquad (4.24)$$

where

$$Z_1 = \frac{\pi}{2E_m} Z$$

and X, Y and Z are defined in equations (4.9), (4.10) and (4.11).

Applying Popov's theorem given in Appendix B, it is required, for the system to be absolutely stable, that there exist a $q \geq 0$ such that

$$\begin{aligned} \mathrm{Re}(1+j\omega q)W(j\omega) = {} & JX\omega^2(-JL_a\omega^2+BR_a+K_vK_t) - \omega^2(BR_a+YK_t+Z_1) \\ & + \{q\omega^2(BX+YK_t+Z_1)(-JL_a\omega^2+BR_a+K_vK_t)\} \\ & + q\omega^4 JX(BL_a+JR_a) \geq 0 \end{aligned} \tag{4.25}$$

If

$$q = -JX/(BX + YK_t + Z_1) \tag{4.26}$$

then eqn.(4.25) reduces to

$$-\frac{\{(BX + YK_t + Z_1)^2 + J^2X^2\omega^2(BL_a + JR_a)\}}{(BX + YK_t + Z_1)} \geq 0 \tag{4.27}$$

If $(BX+YK_t + Z_1) \leq 0$, the above condition is satisfied. Thus the condition

$$\left.\begin{array}{l} X > 0 \\ \text{and} \\ (BX + YK_t+Z_1) < 0 \end{array}\right\} \tag{4.28}$$

will ensure the absolute stability of the system. The numerical values of X and $BX+YK_t+Z_1$ for the system with controller parameters designed in Sec.4.5 are given in

Table 4 1 Design Parameters

Speed controller gain K_{s1}	=	1.109
Speed controller time constant τ_a	=	0 0625
Current controller gain K_1	=	3 656

Table 4.2

Speed in rpm	Load torque in NW-m.	Eigenvalues of the system
1200	2 0	-42, -22, -114 6
	1.0	-32, -27, -165
	0.0	$-28 \pm j5.56$, -206
600	2 0	$-27\ 8 \pm j8.27$, - 290
	1 0	$-27\ 2 \pm j8\ 14$, -282
	0.0	$-27 \pm j8$, -303
300	2.0	$-27\ 8 \pm j8.2$, -286
	1 0	$-27\ 7 \pm j8.6$, -307
	0.0	$-27\ 8 \pm j8\ 4$, -297

Table 4 .3

X = 5 .0982	
$BX+YK_t+Z_1$ = -0.942556	

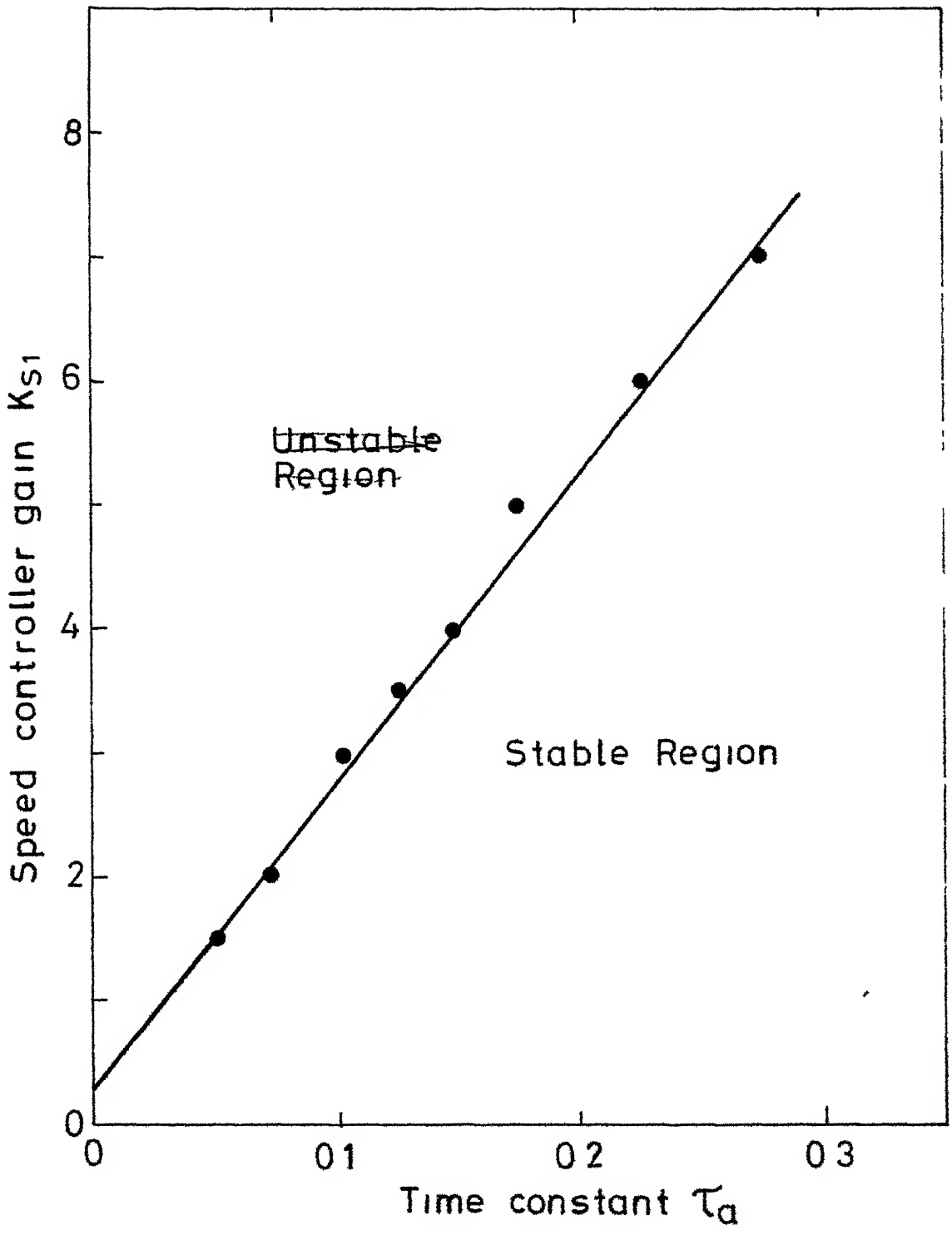

Fig 4 8 b Boundary between stable and unstable regions

Table 4 3 Thus the design ensures absolute stability of the system

The system has been tested with the designed values. Furthermore, the stability boundary in terms of system parameters has also been determined This is shown in Fig 4 8b.

4.7 DIGITAL SIMULATION

Digital simulation of any system is useful at the design stage to predict the behaviour of the system In the present work, the closed loop speed control scheme of converterfed dc motor is simulated. Though the program is written for P-I controller, it can be suitably adapted to any type of control. In the simulation, continuous conduction and discontinuous conduction periods are identified and the dynamics of the system is calculated taking into account both types of discontinuous conduction (Chapter 3) and continuous conduction. If the current is zero and if α_f is less than γ, firing angle α_f is modified as γ because the thyristors cannot be fired as back emf, which is greater than supply voltage acts as a reverse bias on the incoming thyristor. Further, if $\alpha_f < \gamma$ and current is flowing in the incoming thyristor will fire. Now if the current becomes zero before angle γ, then also firing angle will be γ due to reasons mentioned above.

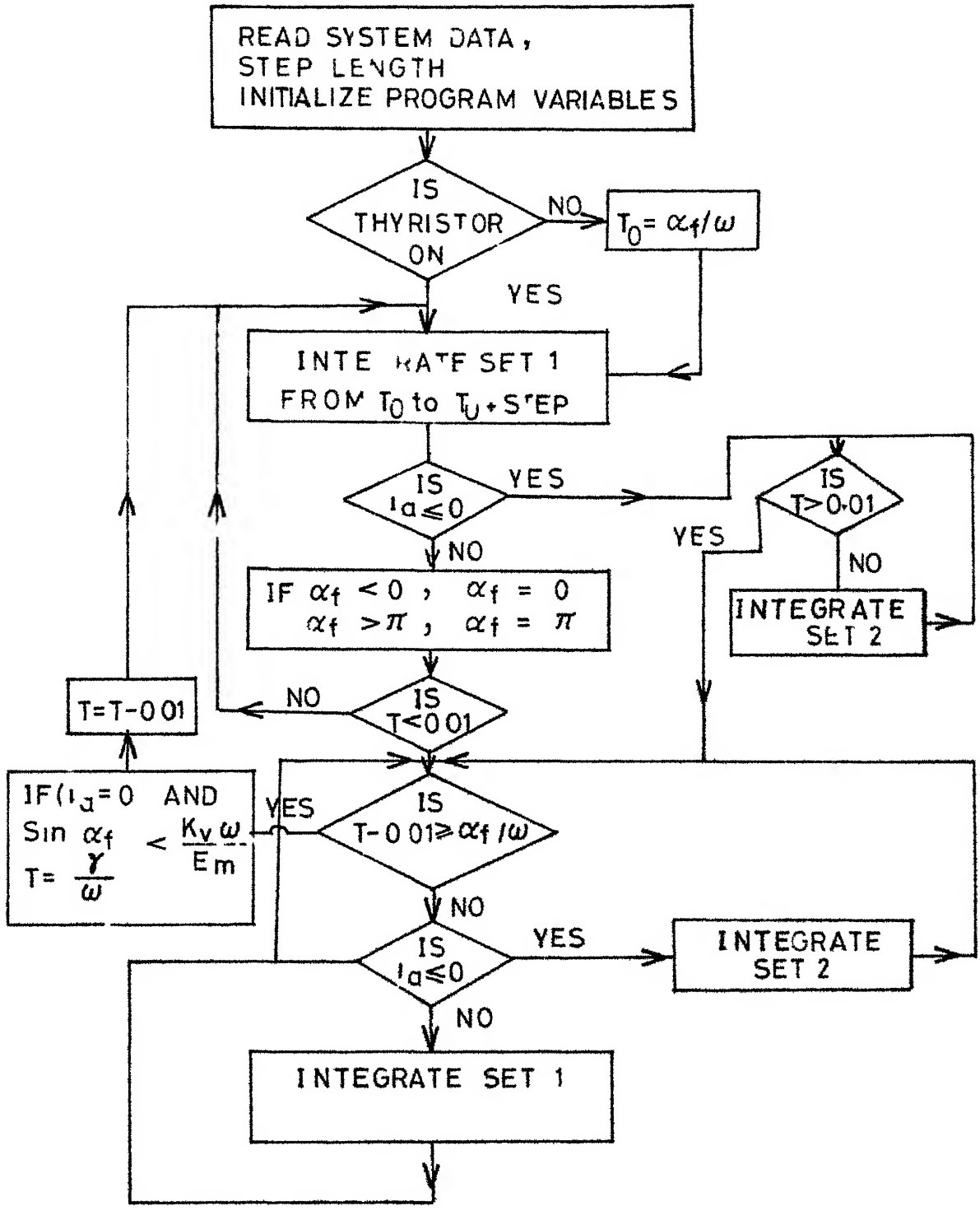

Fig. 4·9 Flow chart for system simulation

During the continuous conduction, the system dynamics is described by the following differential equations

$$\left.\begin{aligned} \frac{di_a}{dt} &= -\frac{R_a}{L_a} i_a - \frac{K_v}{L_a}\omega + U_a \\ \frac{d\omega}{dt} &= \frac{K_t}{J} i_a - \frac{B}{J}\omega - \frac{T_l}{J} \\ \frac{d}{dt}\alpha_f &= A_1 i_a + A_2 \omega + A_3 U_a + A_4 \end{aligned}\right\} \qquad (4.29)$$

where

$$\left.\begin{aligned} A_1 &= \frac{K_l \pi}{V_m}\left(K_{s1} K_{fs} K_t/J - K_{fi} R_a/L_a\right) \\ A_2 &= \frac{K_l \pi}{V_m}\left(K_s K_{fs} - K_{s1} K_{fs} B/J - K_{fi} K_v/L_a\right) \\ A_3 &= \frac{K_l \pi}{V_m}\left(K_{fi}/L_a\right) \\ A_4 &= -\frac{K_l}{V_m}\left(K_{s1} K_{fs} T_l/J + K_s V_{ref}\right) \end{aligned}\right\} \qquad (4.30)$$

In the above equations, $U_a = E_m \sin \omega t$ and at every firing instant, U_a is shifted by π radians as the pair of conducting SCRs change at every firing instant. During discontinuous conduction, the system dynamics is described by

$$\left.\begin{aligned} i_a &= 0 \\ \frac{d\omega}{dt} &= -\frac{B}{J}\omega - \frac{T_l}{J} \\ \frac{d}{dt}\alpha_f &= B_1 \omega + B_2 \end{aligned}\right\} \qquad (4.31)$$

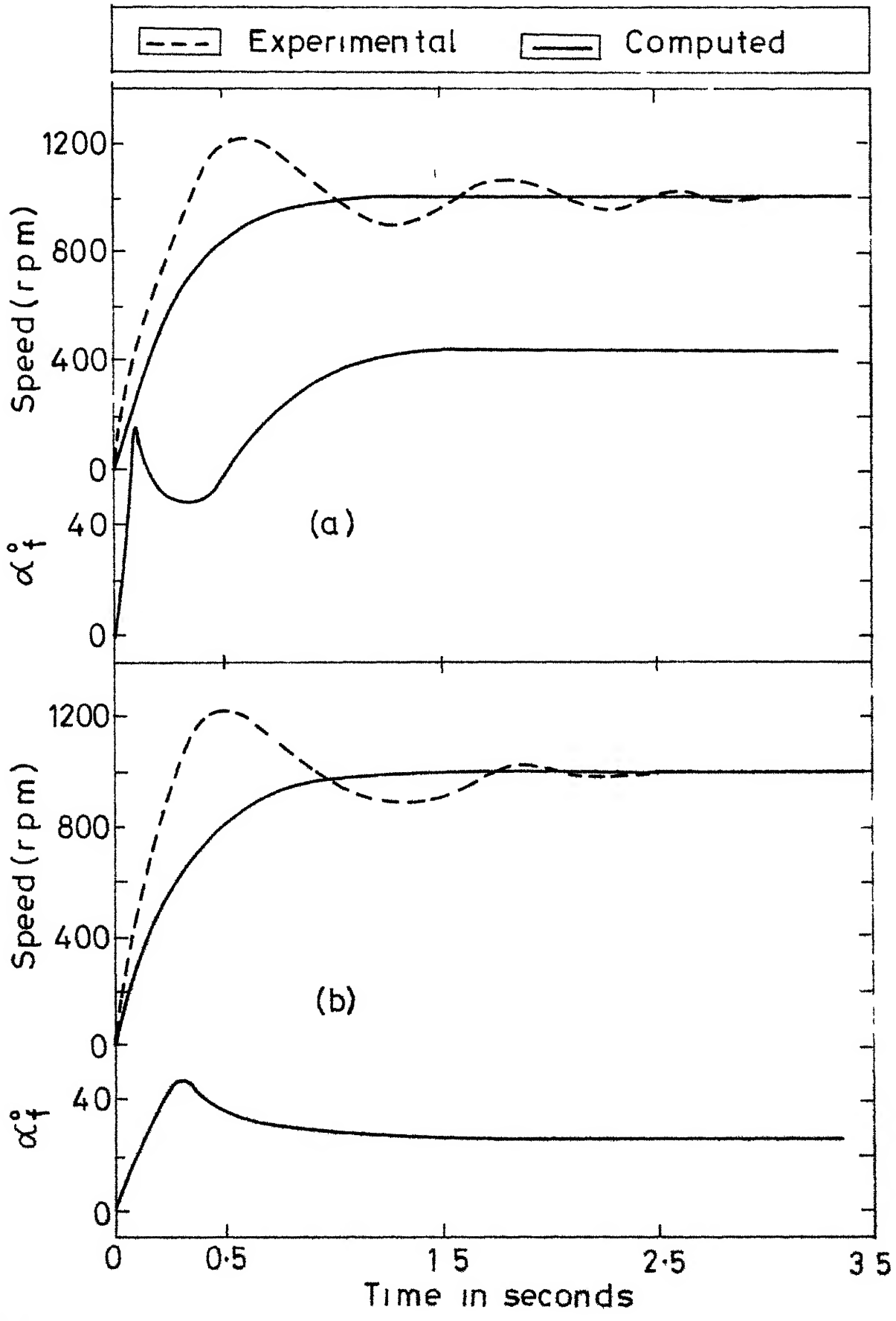

Fig 4 10 Starting transient using PI controller (a) With no load (b) With full load

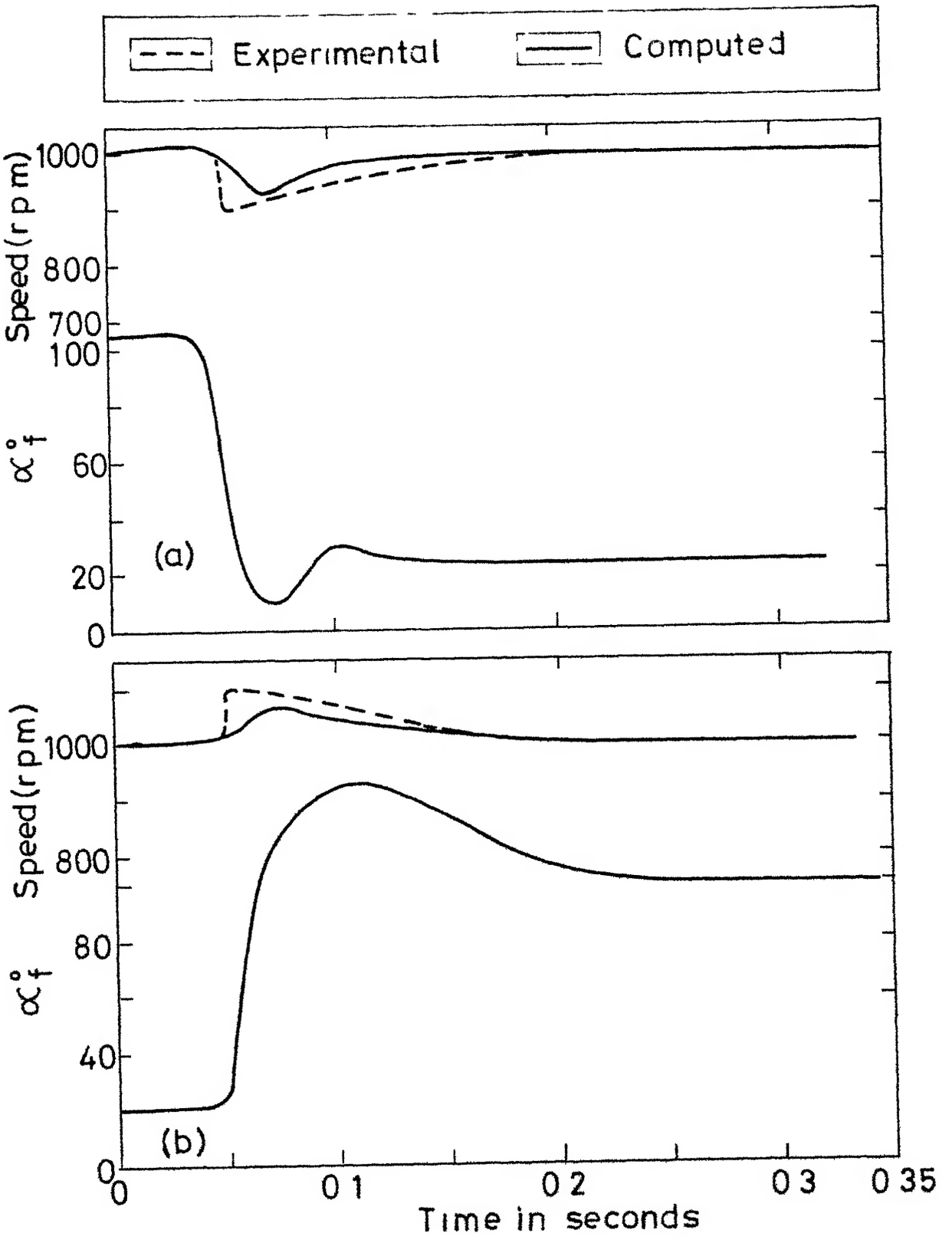

Fig.4 11 Load torque transient with PI Controller step load (a) Applied (b) Thrown off

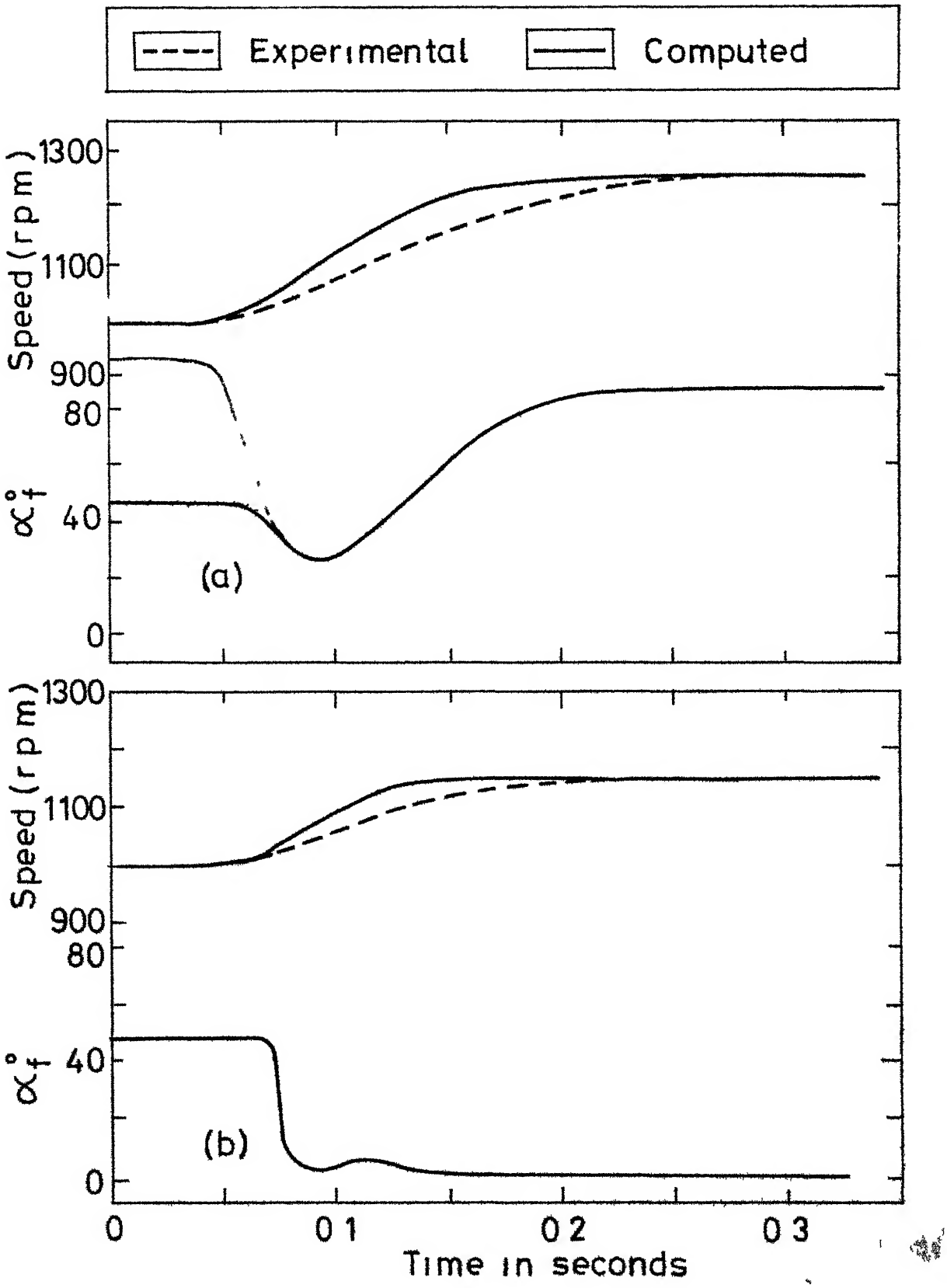

Fig. 4 12 Transient response for increase in V_{ref} with PI controller (a) With no load (b) With full load

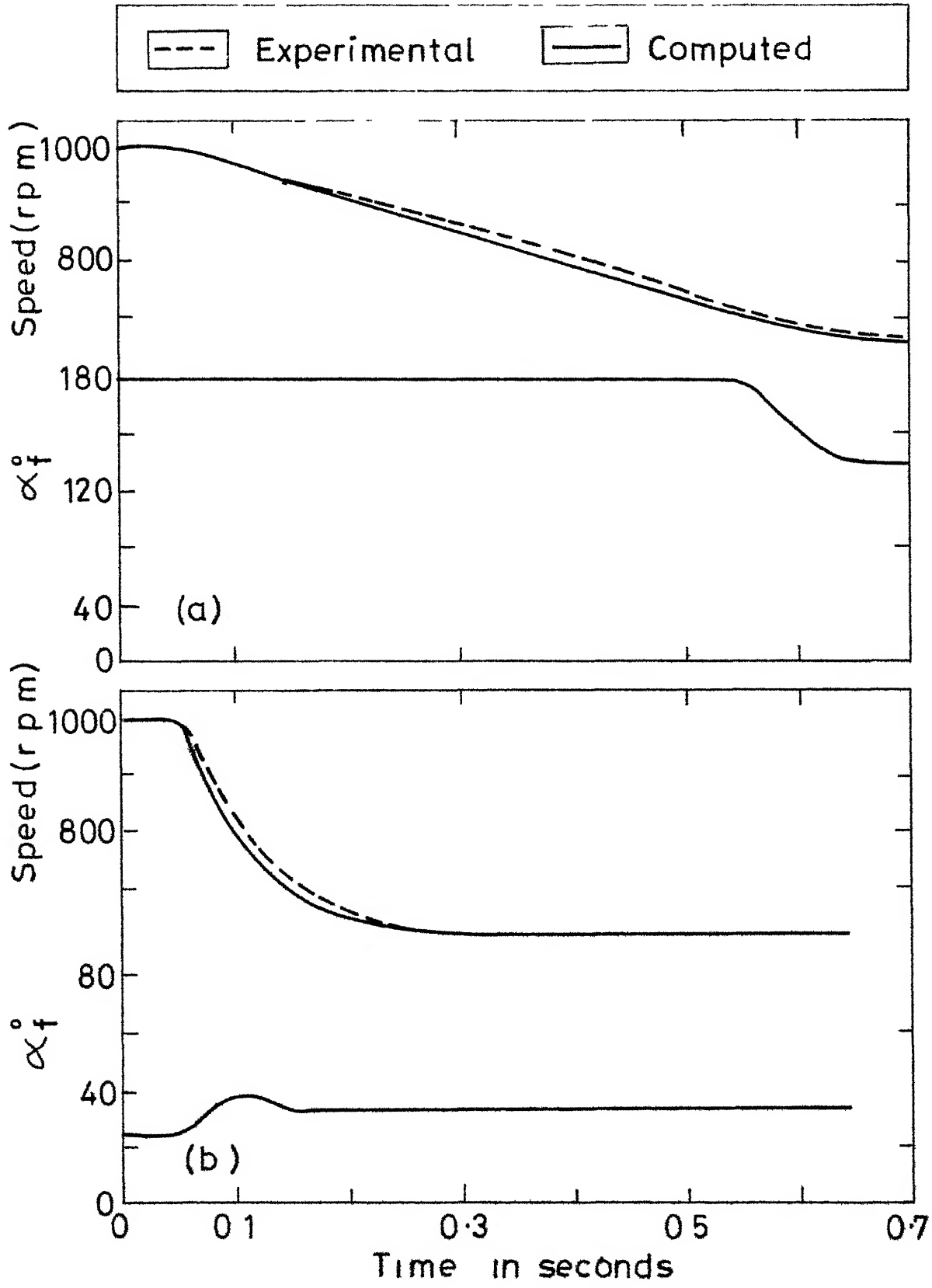

Fig. 4·13 Transient response for decrease in V_{ref} with PI controller (a) With no load (b) With full load

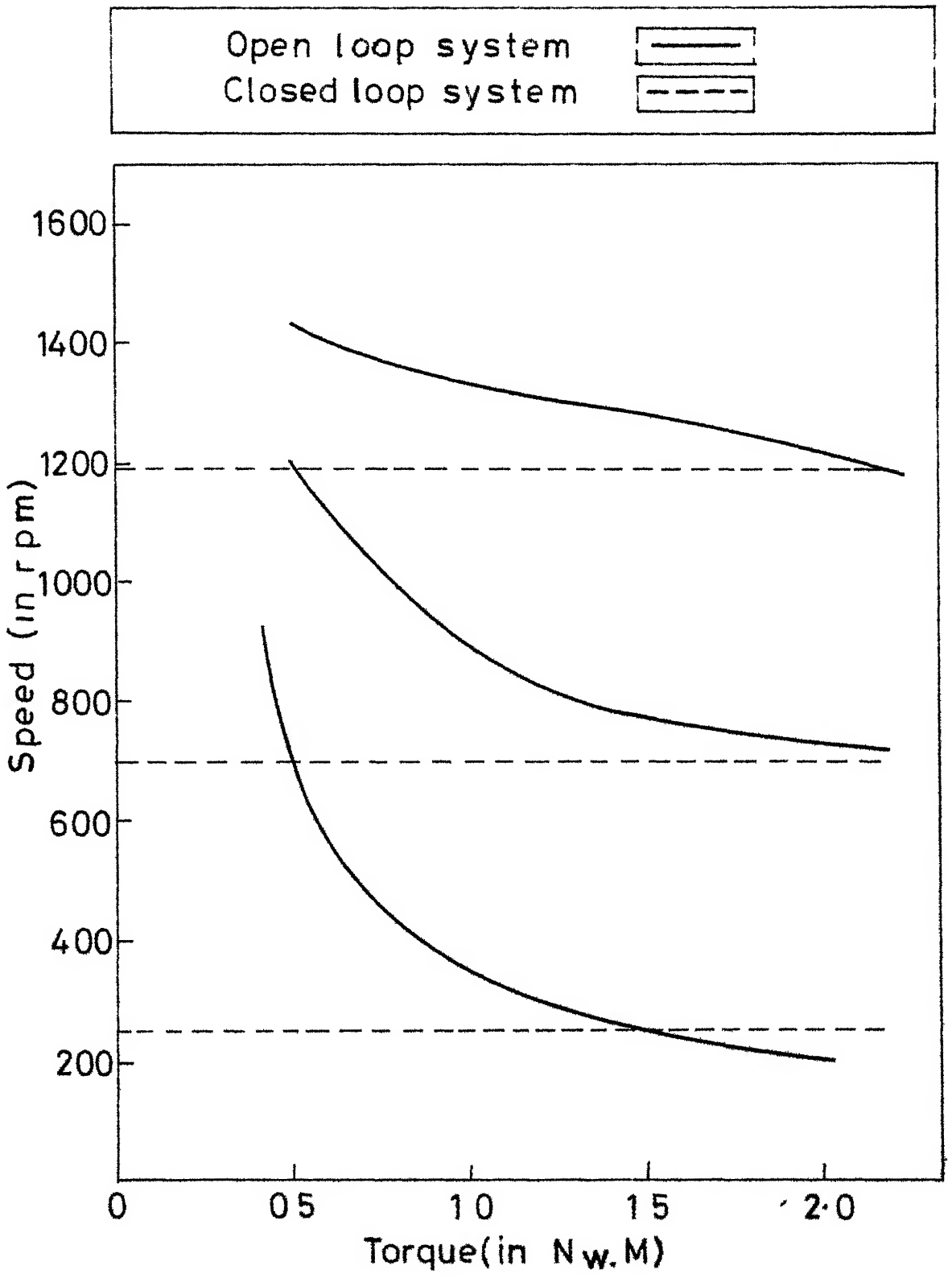

Fig 4 14 Torque speed characteristics

where

$$B_1 = \frac{K_1 \pi}{V_m}(K_s K_{fs} - K_{s1} K_{fs} B/J)$$

$$B_2 = - \frac{K_1 \tau}{V_m}(K_{s1} K_{fs} T_l/J + K_s V_{ref}) \qquad (4.32)$$

The flowchart of the simulation is shown in Fig. 4.9. Numerical integration has been carried out using 4th order Runge-Kutta method.

Transient responses for starting, load torque and V_{ref} changes are shown in Figs. 4.10 to 4.13. Experimental responses are shown with dotted lines. The responses agree well with computed characteristics except in the case of starting transient. In computing starting transient, stiction and Coulomb friction are not taken into account. Viscous friction versus speed is taken as linear which is highly nonlinear when the motor is started from standstill to full speed.

Experimental Results:

Steady state torque speed characteristics are shown in Fig. 4.14. Dotted lines show the torque-speed characteristics for closed loop system. Continuous line shows the torque-speed characteristics for open loop system. The improvement of the closed loop system characteristics over the open loop characteristic is clearly seen.

4.8 STUDY OF AUTO-ADAPTIVE CONTROLLER

Abbot and Wheeler [21] simulated the thyristor dc drive using analog computing elements and logic components for converter switching. Frequency response curves showed wide variation in system dynamics during continuous conduction and discontinuous conduction. To improve the transient performance of the system, two channels were used. P-I controller was used in one channel and proportional controller was used in the other channel. During the current conduction period, P-I controller channel was in action. During zero current period, proportional controller channel was in action.

This chapter describes the results of experimental study and digital simulation of auto-adaptive controller The circuit diagram is shown in Fig.4.15 The part of the circuit marked A has been used to detect the presence or absence of armature current. Analog gate has been used for switching of the channels Experimental results are shown in Fig 4.16 marked with dashed lines. The responses show that the subharmonic oscillations are occurring in the system.

Digital simulation results are shown in Figs. 4.16 to 4.19. In computing the responses, α_f is computed by the following eqn (4.33) during zero current interval.

$$\alpha_f = \pi - \frac{K_1 \pi}{V_m}(K_{s1} V_{ref} - K_{s1} K_{fs} w) \qquad (4.33)$$

The results show that at low torques there is steady state error.

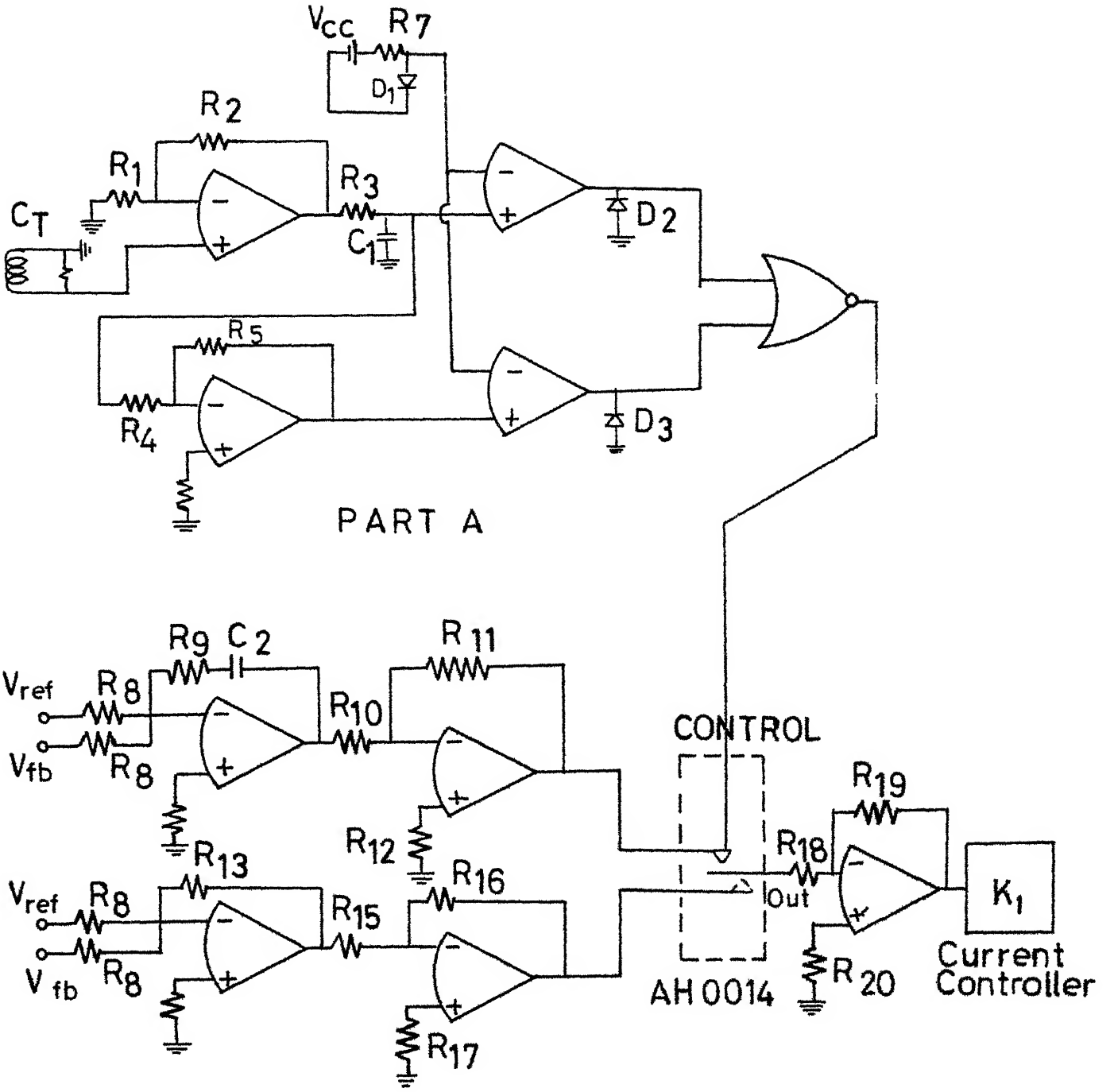

Fig. 4·15 Control circuit for autoadaptive controller

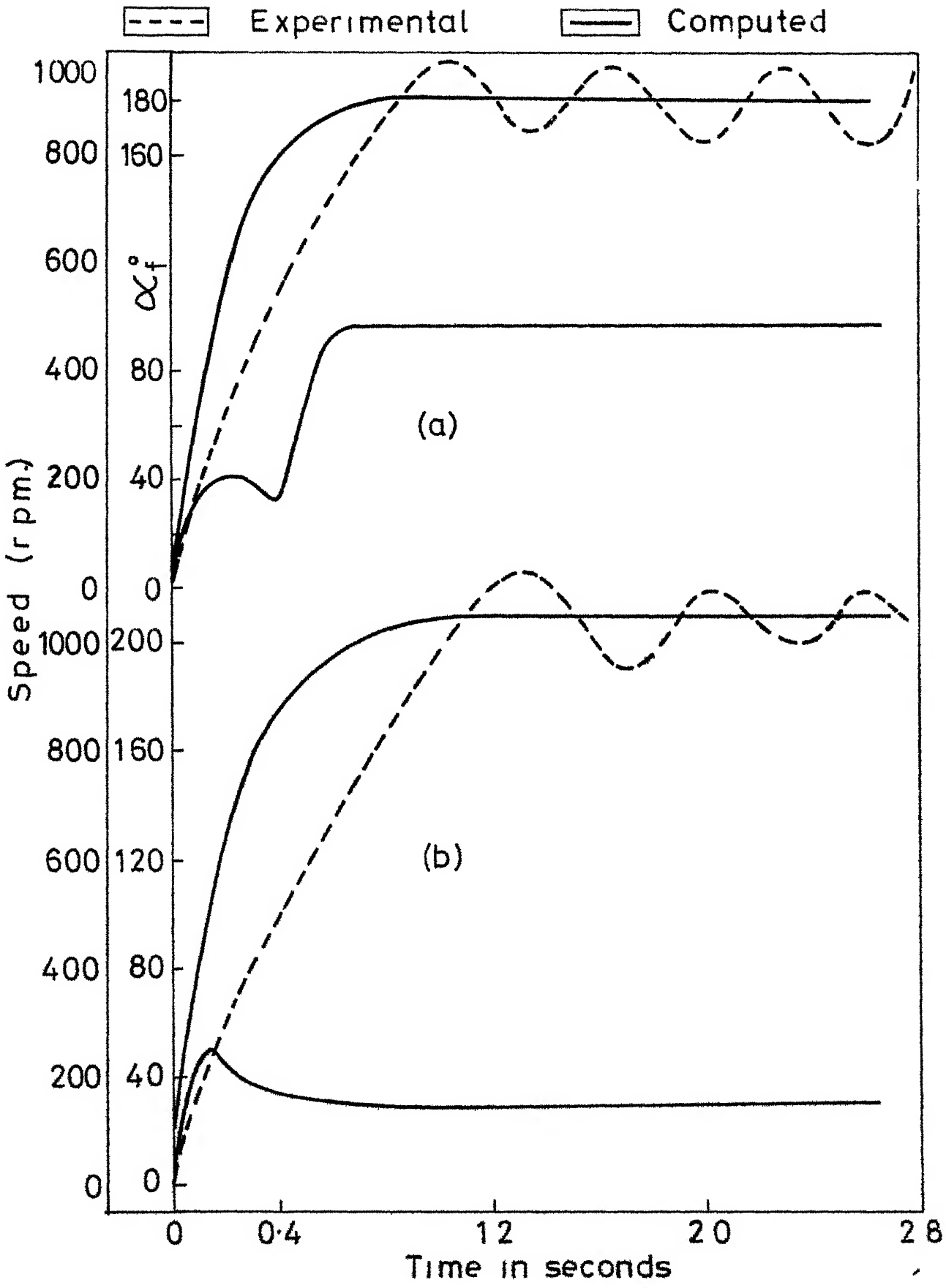

Fig 4 16 Starting transient using adaptive controller with (a)No load (b) Full load

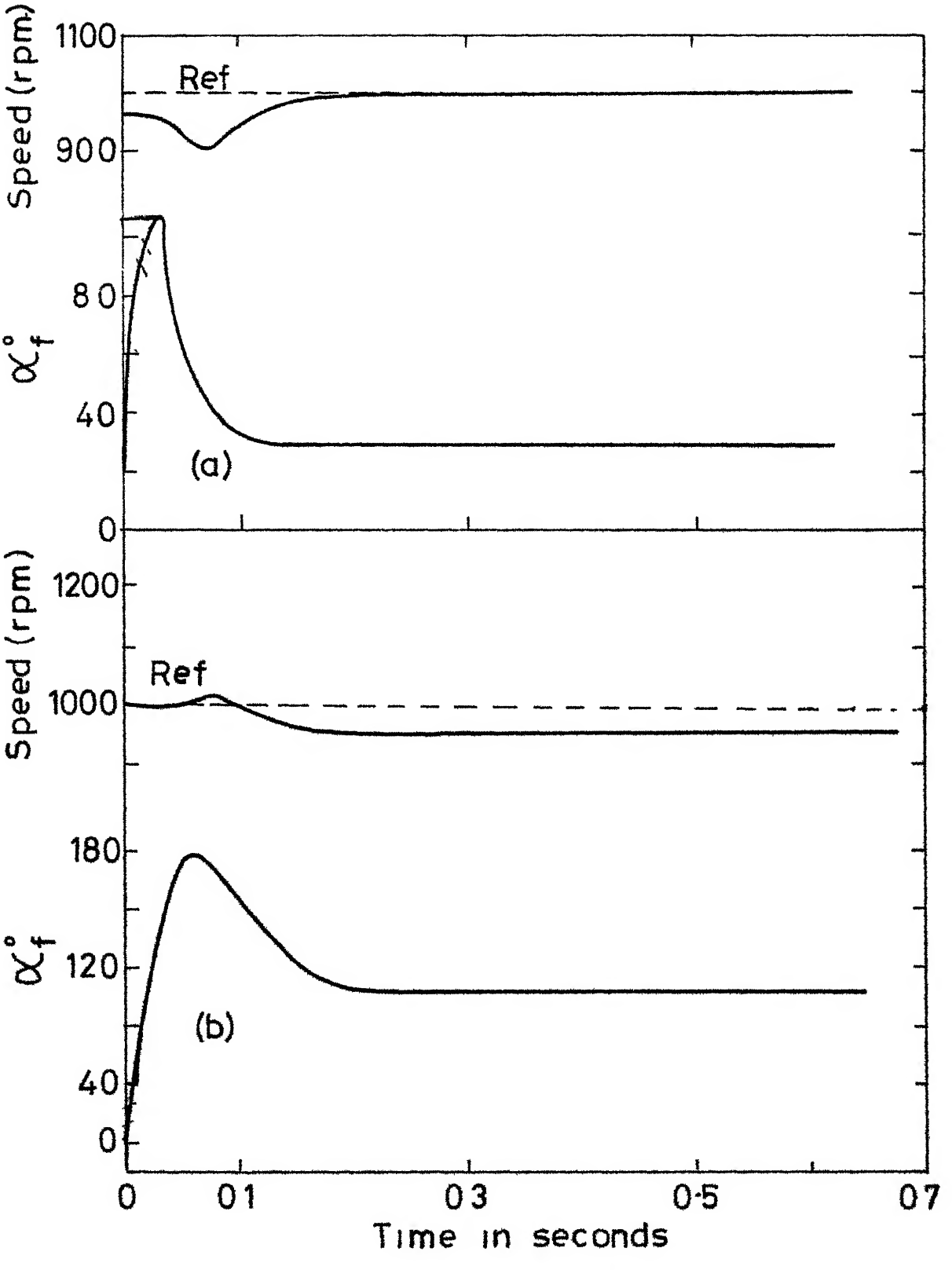

Fig.4·17 Load torque transient with adaptive controller
STEP LOAD (a) Applied (b) Thrown off

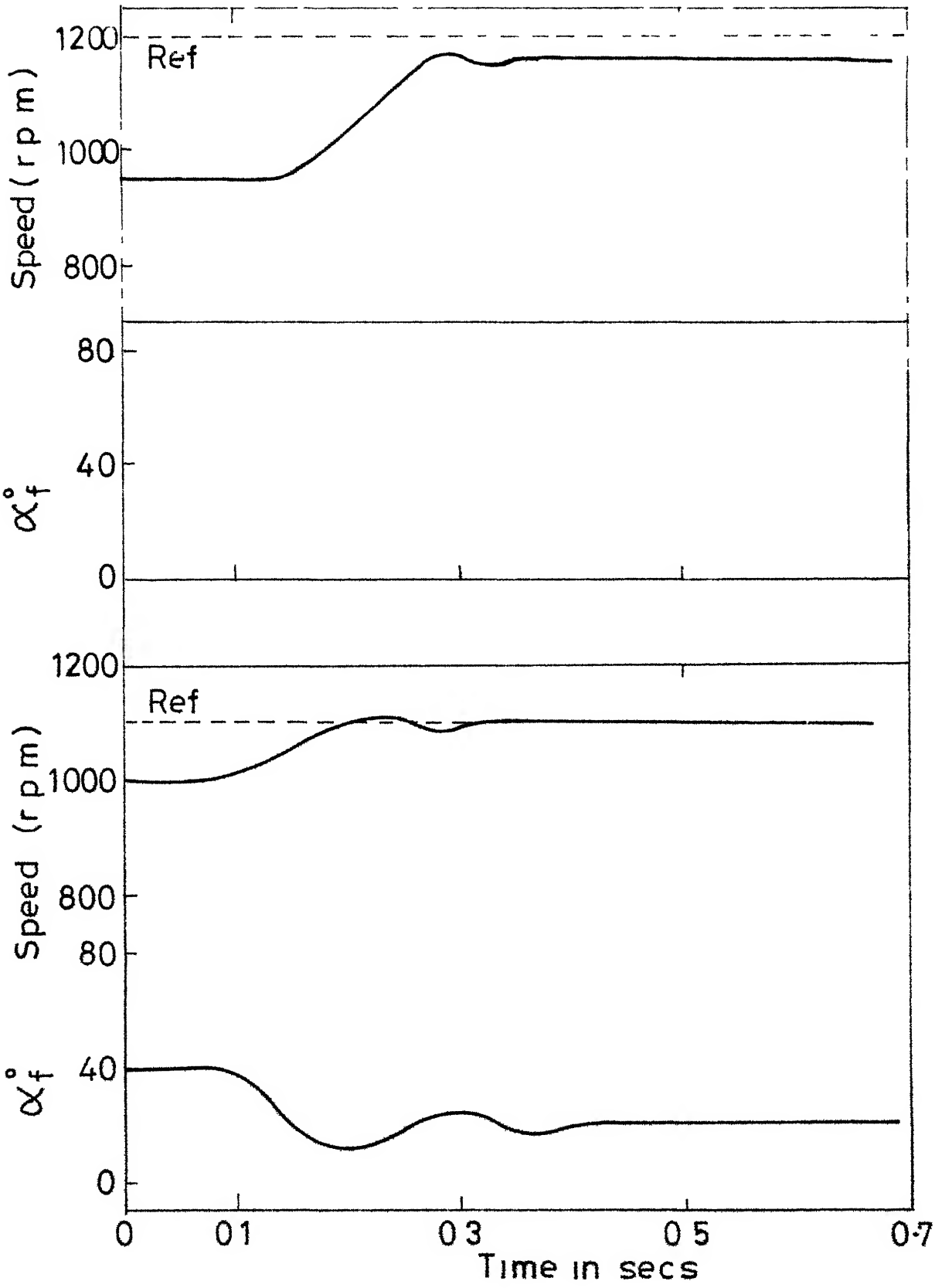

Fig. 4·18 Transient response for increase in Vref (a) With no load (b) With full load

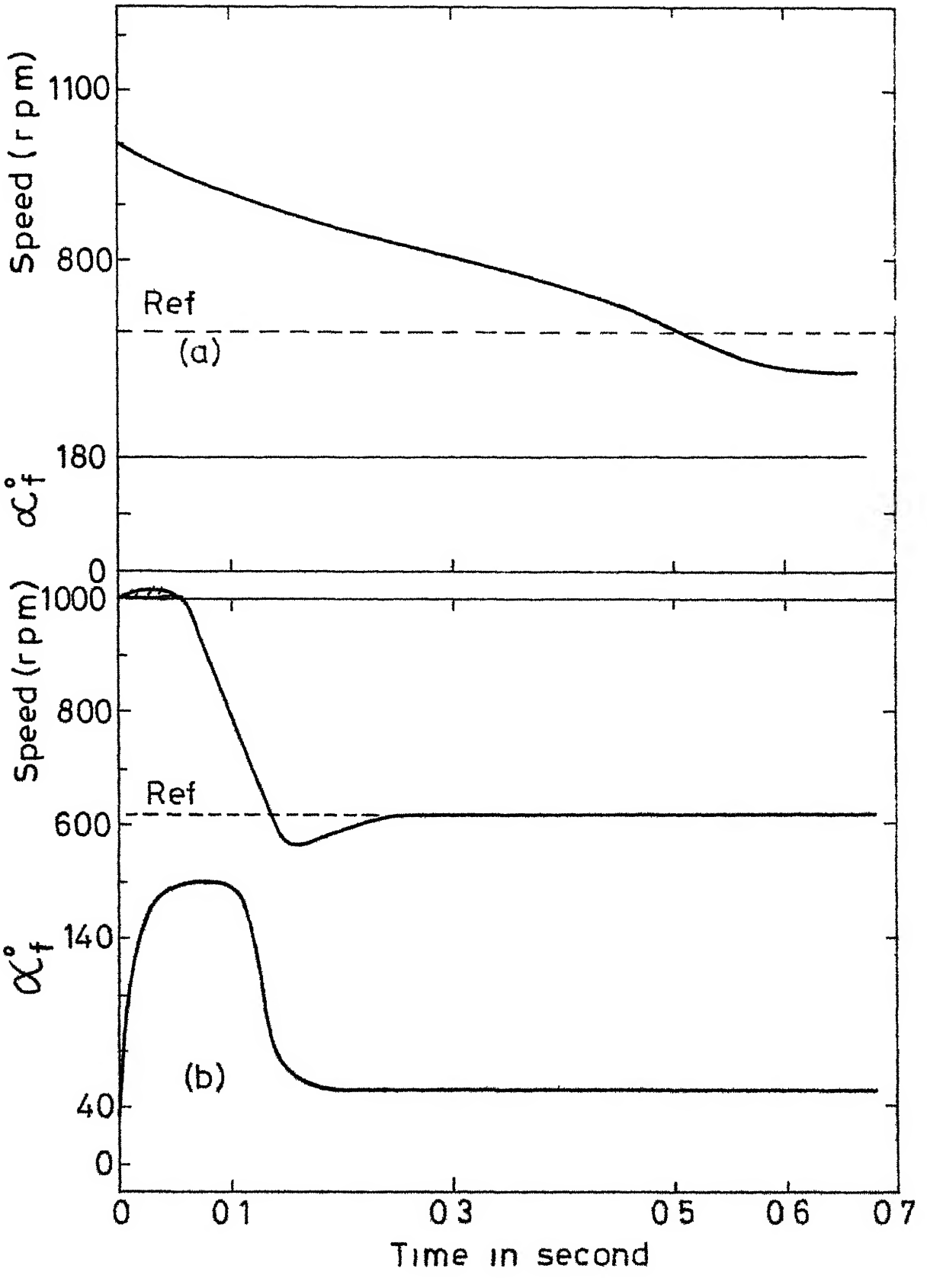

Fig. 4·19 Transient response for decrease in V_{ref} with adaptive controller with (a) No load (b) Full load

But at high torques, there is no steady state error. The reason is that at low torques, discontinuous conduction takes place. Proportional channel will be in action during zero current interval and the firing of the converter is controlled by the proportional controller which contributes to steady state error At high torques, the current is continuous and P-I controller will be in action during that period. Firing of the thyristors is controlled by the P-I controller because of which there will be zero steady state error.

Regarding the transient response, no improvement is seen from the simulation results for the adaptive case. It appears that the adaptive controller suggested by Abbot and Wheeler does not offer advantages in the present situation. In addition, it gives steady state error for lightly loaded conditions.

CONCLUSIONS

The new firing scheme developed here is stable and immune to stray and noise pulses as it does not use components like monostables etc which are sensitive to noise and stray pulses. It can be used for many converter operations such as 1 fully controlled operation, 2.half controlled operation, 3) sequence control, 4 symmetrical pulse width modulation with one pulse per half cycle, 5. asymmetrical triggering control. The method derived here for the calculation of filter inductance which eliminates discontinuous conduction and keeps the ripple within permissible limits can be used either for fully controlled operation or for half controlled operation. The monograms can be used for a motor of any rating as they are given in normalized variables. This method gives an optimum value of inductance which permits the elimination of discontinuous conduction and reduction of ripple to prescribed value with minimum adverse effect on transient response.

The method presented for the design of compensators can be used for the dc drive with closed loop scheme to avoid run away instability as well as ripple instability. The flowchart and the simulation scheme presented are useful at the design stage to predict the behaviour of

the system as it takes into account continuous conduction and both types of discontinuous conduction. It is concluded from the study of auto-adaptive controller that there will be no improvement in the transient performance using auto-adaptive controller over the PI controller. In addition it contributes steady state error at highly loaded conditions

APPENDIX A

DETERMINATION OF MOTOR PARAMETERS

i) The armature resistance is measured by voltmeter-Ammeter method The armature inductance is measured on an impedance bridge.

$$R_a = 27.5 \text{ ohms}$$

$$L_a = 340 \text{ mH}$$

ii) The motor is run as a generator and emf versus speed curve is plotted. From this curve back emf constant K_v is calculated ($E_b = K_v$).

iii) The motor no load input ($E_b I_a$) is measured at various speeds and no load torque versus speed is determined. From this characteristic, the friction coefficient B is calculated At the rated speed of 1200 rpm, the torque developed by the motor for armature currents is determined and the torque coefficient K_t calculated

iv) The motor is run at the rated speed and the input voltage is switched off suddenly. Speed versus time curve is recorded on an X-Y plotter The mechanical time constant T_m is then calculated. The moment of inertia J is calculated as T_m.B.

The parameters of the system thus determined are given in Table A.1. Table A.1 also includes the P-I controller parameters.

Table A 1

Parameter	Value	Parameter	Value
R_a	27 5	K_{s1}	1 .0
L_a	0 6	τ_a	0.06
K_v	1 45	K_1	3.6
J	0.002941	K_{f1}	1.0
B	0 001948	K_{fs}	0.0762
K_t	1 7		

APPENDIX B

POPOV'S STABILITY CRITERION

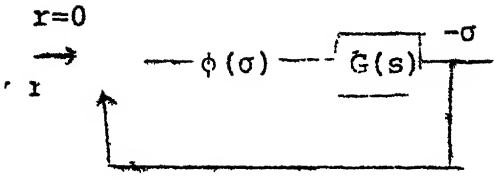

Fig.B.1 Nonlinear System

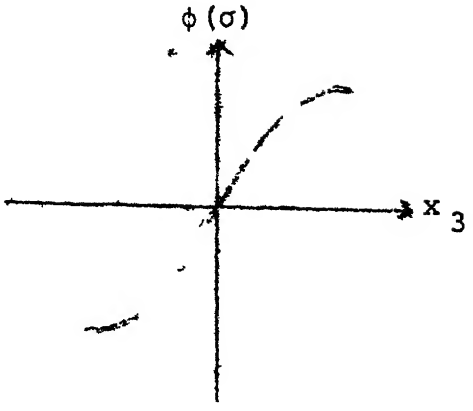

Fig. B.2 Nonlinearity satisfying 'sector condition'

The problem of stability of the system shown in Fig.B.1 has received considerable attention in nonlinear control theory The system equations are

$$\left.\begin{aligned} \dot{\underline{x}} &= A\,\underline{x} + \underline{b}\,y \\ y &= \phi(\sigma) \\ \sigma &= c^T \underline{x} \end{aligned}\right\} \qquad (B.1)$$

where $\underline{x}$ is the n-dimensional state vector, A is an nxn matrix, b and c are n-dimensional vectors and $\phi(\sigma)$ is a memoryless time invariant continuous nonlinear function satisfying the sector condition (Fig B.2).

$$\sigma\,\phi(\sigma) > 0 \text{ for all } \sigma \neq 0$$
$$\phi(\sigma) = 0 \text{ for } \sigma = 0\ . \qquad (B.2)$$

In (B.1), the case where matrix A has one zero eigenvalue and all other eigenvalues in the open left half plane is referred to as the simplest particular case in control theory literature, and the system considered here falls into this category.

The transfer function of the linear part is obtained as

$$G(s) = -\underline{c}^T(sI-A)^{-1}\,\underline{b} \qquad (B.3)$$

The global asymptotic stability of the equilibrium state $\underline{0}$ of system (B.1) for the class of nonlinear functions satisfying condition (B.2) is termed absolute stability in the finite sector $(0, \infty)$

Popov's Theorem

System (B.1), with A having one zero eigenvalue and all other eigenvalues in the open left half-plane, is absolutely stable in $(0, \infty)$ if there exists a real number $q \geq 0$ such that

$$\mathrm{Re}(1+qj\omega)\,G(j\omega) \geq 0 \quad \text{for all real } \omega > 0 \qquad (B.4)$$

The inequality (B.4) is called the Popov's condition.

REFERENCES

1. SCR Manual, New York, GEC 1967.

2 J Millman and H. Taub, Pulse Digital and Switching Waveforms Kogakshsha, Mc-Graw-Hill 1967, pp. 422-431

3 W N Cheung, "Pulse delay circuits suitable for triggering thyristors", Electronic Engineering, pp.211-213, Feb.1969.

4 R Arockiasamy and S Doriapandy, "A novel scheme to obtain voltage controlled time delay suitable for thyristor control", IEEE Trans IECI, Vol.23, No 1, Feb.1976.

5 A Yair and M. Steinkoler, 'Improved pulse delay circuit for phase controlled rectifiers and ac voltage controllers", IEEE Trans IECI, Vol , May 1977, p.200

6 W. Farrer and D F Andrew, "Fully controlled regenerative bridges with half controlled characteristics", Proc. IEE, Vol.125, No 2, 1978, pp. 109-112

7. I. Mehta and S Mukopadhyay, 'Improvement in dc motor performance by asymmetrical triggering', Part I - one quad drive, IEEE Trans IA, Vol.IA-2, 1975, pp 172.

8 I C Sen and S R. Doradla, "Symmetrical and extinction angle control of solid state series motor drive", IEEE Trans. IECI, Vol.23, 1976,pp. 31-38.

9, "A three-phase universal controller", Philips, Electronic Appl. News, Vol.15, No 4, July/Aug 1978, pp.42-48.

10 P Mehta and S. Mukopadhyay, "Modes of operation on converter controlled dc drives', Proc. IEE, Vol 121, No 3, pp 179-183, March 1974.

11. C.E. Robinson, "Redesign of dc motors for application with thyristor power supplies", IEEE Trans. IGA-4, 1968, pp508-514.

12 F I. Edwin and G K. Dubey, "Transient analysis of converter controlled dc separately excited motor". J Electric Machines and Electromechanics, 1978, pp. 385-402

13 K G. Black, "The effect of rectifier discontinuous current on motor performance", IEEE Trans. IGA, 1964, pp 377-382.

14. G K. Dubey, "Calculation of filter inductance for chopper fed dc separately excited motor", Proc. IEEE, Vol.66, No.12, 1978, pp. 1671-73

15. V. Subbaiah and S Palanichamy, "Mode identification and minimum inductance estimation forfully controlled thyristor converters", IEEE Trans IECI, Vol.26, Feb.1979, pp 48-50

16. T Krishnan and Ramaswamy, "A fast response dc motor speed control system", IEEE Trans. IA, Vol IA-10, No.5, Sept./ Oct 1974, pp 643-651.

17 M.A Pai, M. Ananda Mohan and J Gopala Rao, "Power system transient stability regions using Popov's method', IEEE Trans PAS, Vol 89, No 5, May/June 70, pp. 788-794.

18. G K Dubey and S R. Doradla, "Intensive Course on Solid State Power Controls at Bhilai Tech.Institute", 1978.

19. M J Nieniwski and Richard S Morkau, "Digital simulation of an SCR driven DC motor", IEEE Trans. IA, Vol.14, No.4, July/Aug 1978,

20. N K. De and A K Chatopadhyay, "Modelling an SCR bridge", IEEE Trans. IECI, May 1978, pp. 187-89.

21. K.M. Abbot and J D Wheeler, "Simulation and control of thyristor drives", IEEE Trans IECI, Vol.25, No.2, May 1978, pp. 130-137.

22. Farag, Malik and Hope, "Studies on an SCR controlled variable speed dc shunt motor, IEEE Trans. PAS, May/June 1974.